Bioactive Materials 41 (2024) 355–370

Contents lists available at ScienceDirect

Bioactive Materials

journal homepage: www.keaipublishing.com/en/journals/bioactive-materials

An anti-senescence hydrogel with pH-responsive drug release for mitigating intervertebral disc degeneration and low back pain

Wantao Wang [a,b,c,1], Lei Liu [c,1], Wenzheng Ma [a,b,c,1], Lei Zhao [c], Lin Huang [c], Dan Zhou [c], Jinghao Fan [c], Jianru Wang [a,b], Hongmei Liu [c,**], Decheng Wu [c,***], Zhaomin Zheng [a,b,*]

[a] Department of Spine Surgery, The First Affiliated Hospital, Sun Yat-sen University Guangzhou, 510080, People's Republic of China
[b] Pain Research Center, Sun Yat-sen University, Guangzhou, 510080, People's Republic of China
[c] Guangdong Provincial Key Laboratory of Advanced Biomaterials, Department of Biomedical Engineering, Southern University of Science and Technology, Shenzhen, 518055, People's Republic of China

ARTICLE INFO

Keywords:
Intervertebral disc degeneration
Low back pain
Senescence
Quercetin
Hydrogel

ABSTRACT

Oxidative stress and aging lead to progressive senescence of nucleus pulposus (NP) cells, resulting in intervertebral disc (IVD) degeneration (IVDD). In some cases, degenerative IVD can further cause low back pain (LBP). Several studies have confirmed that delaying and rejuvenating the senescence of NP cells can attenuate IVDD. However, the relatively closed tissue structure of IVDs presents challenges for the local application of anti-senescence drugs. Here, we prepared an anti-senescence hydrogel by conjugating phenylboronic acid-modified gelatin methacryloyl (GP) with quercetin to alleviate IVDD by removing senescent NP cells. The hydrogel exhibited injectability, biodegradability, prominent biocompatibility and responsive release of quercetin under pathological conditions. In vitro experiments demonstrated that the hydrogel could reduce the expression of senescence markers and restore the metabolic balance in senescent NP cells. In vivo studies validated that a single injection of the hydrogel in situ could maintain IVD tissue structure and alleviate sensitivity to noxious mechanical force in the rat models, indicating a potential therapeutic approach for ameliorating IVDD and LBP. This approach helps prevent potential systemic toxicity associated with systemic administration and reduces the morbidity resulting from repeated injections of free drugs into the IVD, providing a new strategy for IVDD treatment.

1. Introduction

Low back pain (LBP) is a highly prevalent clinical health issue, serving as a significant contributor to global disability and imposing substantial healthcare expenditures on society [1,2]. Intervertebral disc (IVD) degeneration (IVDD) is considered the primary cause of LBP, which refers to the physiological and pathological process of natural degeneration and aging of IVD [3]. However, the current clinical treatments for IVDD including conservative treatments and surgical interventions focus on alleviating pain and symptoms rather than arresting progression of IVDD or restoring disc function [4]. Thus, there exists an unmet clinical need to discover efficacious strategies for delaying the progression of IVDD and/or regenerating the degenerated IVD in order to ultimately accomplish the objective of managing low back pain.

The IVD is composed of the annulus fibrous (AF), cartilage endplate (CEP) and highly hydrated nucleus pulposus (NP). The gelatinous NP consists of proteoglycans and type II collagen (Col II), which can support the disc to withstand various mechanical pressures during different activities. Therefore, a decrease in NP function is considered to be the main pathological basis of IVDD [5]. The dysfunction of NP is associated with

Peer review under responsibility of KeAi Communications Co., Ltd.
* Corresponding author. Department of Spine Surgery, The First Affiliated Hospital, Sun Yat-sen University, Guangzhou, 510080, People's Republic of China.
** Corresponding author.
*** Corresponding author.
E-mail addresses: justtt0317@163.com (W. Wang), liul3@sustech.edu.cn (L. Liu), doctormwz@163.com (W. Ma), 12232575@mail.sustech.edu.cn (L. Zhao), huanglin_chem@163.com (L. Huang), 12231186@mail.sustech.edu.cn (D. Zhou), 12031291@mail.sustech.edu.cn (J. Fan), wangjru@mail.sysu.edu.cn (J. Wang), liuhm@sustech.edu.cn (H. Liu), wudc@sustech.edu.cn (D. Wu), zhzhaom@mail.sysu.edu.cn (Z. Zheng).
[1] Wantao Wang, Lei Liu and Wenzheng Ma contributed equally on this manuscript.

https://doi.org/10.1016/j.bioactmat.2024.07.031
Received 14 March 2024; Received in revised form 27 June 2024; Accepted 22 July 2024

both age-related change and tissue damage caused by multiple stresses. Emerging evidence from clinical and animal researches indicates that senescent IVD cells, especially senescent NP cells, increase in aging and degenerated IVD, representing a novel hallmark and significant contributor of IVDD [5–7].Cellular senescence is a process in which different triggers (including DNA damage, telomere dysfunction, increased reactive oxygen species, etc.) lead to gradual decreases in cell proliferation, differentiation and physiological functions during life activities [8]. In the context of IVDD, senescent NP cells within discs may contribute to the degradation of extracellular matrix (ECM) components, such as proteoglycans and collagen, leading to a decrease in disc height and altered biomechanical properties [9,10]. Additionally, senescent NP cells secrete proinflammatory molecules, a phenomenon often referred to as the senescence-associated secretory phenotype (SASP) [11]. The SASP can contribute to local inflammation within the IVD, further exacerbating degenerative processes [12]. Recently, an increasing number of scholars have started to focus on the repair of IVDD by delaying the senescence process of NP cells. A previous study demonstrated that systemic elimination of senescent cells effectively mitigated age-related IVDD [13]. Similarly, another research confirmed that inhibiting p16 expression of NP cells attenuates IVDD by promoting cell cycle and inhibiting cell senescence [14]. The findings of these studies suggest that targeting senescent NP cells presents a promising therapeutic strategy for delaying IVDD.

Quercetin, a natural flavonoid, is widely distributed in the plant and exhibits potent biological effects [15,16]. Preclinical studies have shown that quercetin can reduce the expression of senescence markers and has a protective effect on a variety of degenerative diseases [17,18]. Several experiments have also confirmed that quercetin can protect NP cells from damage caused by various stimuli [19,20]. However, the administration of senolytic drugs via oral or intravenous routes may encounter significant challenges in the treatment of IVDD. First, due to the fact that NP is an avascular tissue, its nutrient acquisition mainly relies on the diffusion of the CEP and the supply of the AF [21]. As a result, when administered systemically, only a few drugs can be delivered to IVD. A previous trail speculated that oral quercetin 100 mg/kg for treatment would result in a drug concentration of only 2.2–4.0 μg/mL in the IVD [20]. Second, the systemic administration of quercetin may potentially induce side effects due to the formation of o-quinone/quinone methide [22]. On the other hand, local injection of free drugs, which requires the assistance of local anesthesia and imaging guidance, has been associated with problems such as short duration of effective drugs and aggravation of IVDD by repeated injections [23]. Consequently, the development of a drug delivery and sustained-release system adapted for IVDD is urgently needed to locally prolong the action time of quercetin and improve the drug efficacy.

The utilization of biomaterials for constructing local drug delivery systems has garnered increasing interest, aiming to achieve sustained therapeutic drug levels while minimizing the necessity for repetitive injections [24]. Additionally, certain biomaterials used in these systems exhibit the potential to promote IVD regeneration, offering a promising and viable solution for IVDD repair. The NP tissue is a highly hydrated and gelatinous tissue. Given the similarities in composition and mechanical properties between hydrogels and natural NP, hydrogels are considered as ideal materials for repairing NP tissue [24]. Moreover, the injectable hydrogel can adapt to irregularly shaped defects and fully contact with surrounding tissues [25,26]. Among them, gelatin, the hydrolysate of collagen, is a key component of the ECM and exhibits excellent biocompatibility and chemical modifiability, enabling it to mimic collagen-like functions in vitro. Gelatin methacryloyl (GelMA), a photosensitive and injectable hydrogel, can provide a suitable microenvironment and biological matrix for cell life activities and shows good repair effect in IVDD [27]. However, the pathological microenvironment of degenerative IVD undergoes dynamic changes [28,29]. Ossification of the CEP impairs nutrient transport. Consequently, the hypoxic microenvironment induces anaerobic metabolism in NP cells, and continuous hypoxia and glycolysis contribute to lactate accumulation, resulting in a decreasing pH in the IVD. Therefore, the development of a hydrogel system that can release therapeutic drugs in response to the degenerative IVD microenvironment holds an excellent therapeutic prospect. Phenylboric acid (PBA) is a classical Lewis acid that can form a dynamic borate ester bond with the o-phenol structure of quercetin. This reversible covalent bond polymerizes under neutral or alkaline conditions and decomposes under acidic conditions [30]. The decreasing pH in degenerative IVD is conducive to the decomposition of borate bonds between PBA and quercetin, resulting in the responsive release of quercetin.

In this study, we synthesized phenylboric acid modified gelatin methacryloyl (GP) by grafting PBA group onto GelMA. Then we utilized the covalent binding between PBA and quercetin to fabricate an anti-senescence hydrogel loaded with quercetin for the purpose of delaying IVDD. GelMA is functionalized with PBA groups to boost drug loading capacity and enable the hydrogel to release quercetin in response to the pH decreasing microenvironment of the degenerative IVD. The drug loading capacity, injectability, biocompatibility, and pH-responsive drug release characteristics of the hydrogel were initially assessed. Subsequently, we evaluated the effect of the hydrogel on the senescence of NP cells in both oxidative stress and replicative senescence model. Finally, we established an in vivo IVDD model using the puncture method to evaluate the therapeutic efficacy of the hydrogel. Additionally, a rat model of LBP was further constructed to assess the effectiveness of the hydrogel in alleviating LBP induced by IVDD. The schematic diagram was illustrated in Scheme 1.

2. Materials and methods

2.1. Materials

Gelatin type A (924504), methacrylic anhydride (276685), succinic anhydride (239690), 3-aminobenzeneboronic acid (APBA, 900988), 2-hydroxy-1-[4-(2-hydroxyethoxy)-phenyl]-2-methyl-1-propanone (Irgacure 2959), 2-(*N*-morpholino)-ethanesulfonic acid hemisodium salt (MES, V900310), *N*-(3-(dimethylamino)-propyl)-*N*′-ethylcarbodiimide hydrochloride (EDC, E7750), *N*-hydroxysuccinimide (NHS, 130672), bovine serum albumin and quercetin (Q4951) were purchased from Sigma-Aldrich (Darmstadt, Germany). Dulbecco's Modified Eagle Medium (DMEM, C11885500BT), and penicillin/streptomycin (15140122) were purchased from Gibco (Waltham, USA). Fetal bovine serum (FSP500) was purchased from ExCell Bio. (Suzhou, China).

2.2. Synthesis of phenylboronic acid-modified gelatin methacryloyl (GP)

The synthetic synthesis steps of GP were shown in Fig. 1a. The first step was to synthesize GelMA based on previously published reports [31]. Briefly, 1 g of gelatin was dissolved in 10 mL of phosphate buffered saline (PBS) solution at 50 °C, followed by adding 2 mL of methacrylic anhydride and stirring for 1 h. The reaction solution was transferred to a dialysis membrane (7000 Da), dialyzed in deionized water for 5 days, and then lyophilized to obtain GelMA sponge. In the second step, as reported in the literature, the amino groups of GelMA were further converted to carboxyl groups to improve the grafting efficiency of APBA onto GelMA [32]. Briefly, 1 g of GelMA was dissolved in 20 mL of PBS solution at 50 °C, followed by the addition of 0.5 g of succinic anhydride and 1 mL of triethylamine. After being stirred overnight, the mixture was transferred to a dialysis membrane (7000 Da), dialyzed in deionized water for 5 days, and then freeze-dried to obtain carboxylated gelatin methacryloyl (GelMA-COOH). In the third step, 1 g of GelMA-COOH was dissolved in 20 mL of MES buffer (0.1M, pH = 5.5) at room temperature. Then 0.29 g of EDC and 0.17 g of NHS were added and stirred for 20 min to activate the carboxyl groups. The mixture was supplemented with 0.2 g of APBA and stirred at room temperature for 24 h. Subsequently, the resulting solution was transferred to a dialysis membrane (7000 Da),

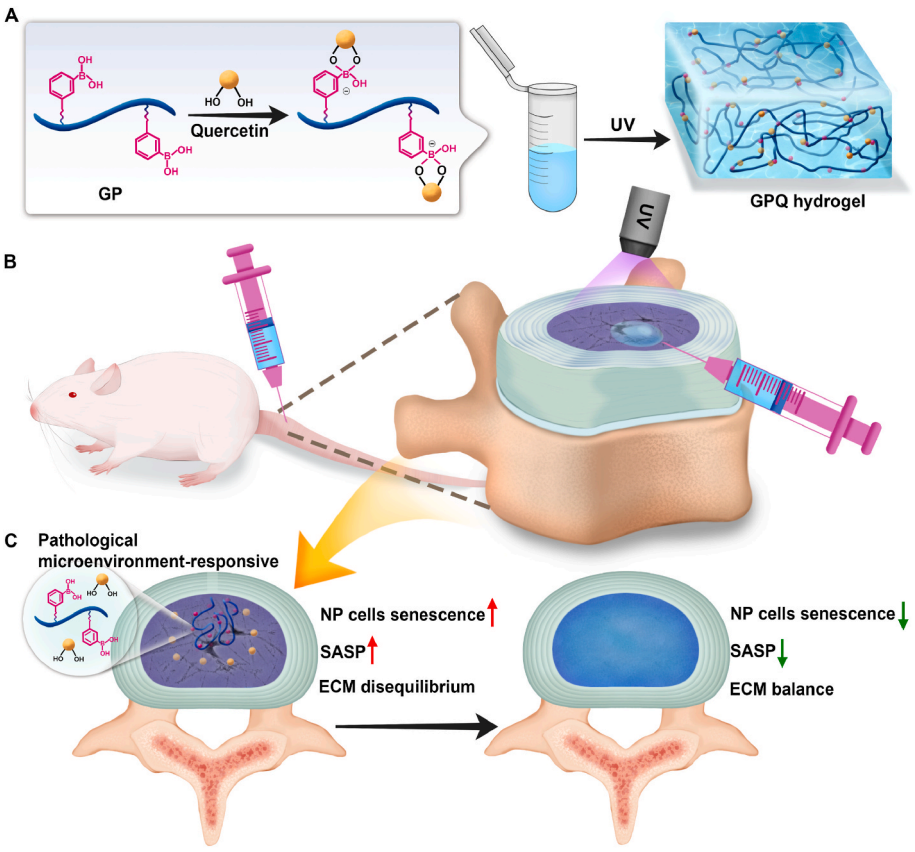

Scheme 1. Schematic illustrations of the GPQ hydrogel and its application in treating degenerative IVD tissue. (A) Synthetic procedures of the GPQ hydrogel. (B) In situ injection therapy in the rat IVDD model. (C) The proposed mechanism of IVD repair.

dialyzed in deionized water for 5 days, and lyophilized to obtain GP.

2.3. Characterization of GP

To confirm the successful modification of gelatin, GelMA and GP were dissolved in PBS solution with a final concentration of 0.01 wt/v%. The absorbance of the solution was measured using a UV spectrophotometer (Shimadzu, Kyoto, Japan) in the wavelength range of 200–500 nm. In addition, GelMA and GP were dissolved in deuterium oxide at a concentration of 10 mg/mL. The hydrogen nuclear magnetic spectrum (^{1}H NMR) spectra was obtained using a 400 Mhz spectrometer (Bruker, Billerica, USA).

2.4. Drug loading of quercetin in GP solution

To calculate the drug loading of quercetin in GP solution, we first dissolved 1 mg of quercetin in 1 mL of dimethyl sulfoxide (DMSO, D103276, Aladdin, Shanghai, China) and then diluted it to 0–100 μg/mL with PBS solution. The absorbance of the solution was measured using a UV spectrophotometer in the wavelength range of 200–650 nm. The absorbance of quercetin solutions at different concentrations was then measured at the wavelength of maximum absorbance in the spectrum, and the standard curve of quercetin was calculated at this wavelength. Subsequently, 1 mg of quercetin was added in 1 mL of PBS solution, 10 wt% GelMA solution and 10 wt% GP solution, respectively. Ultrasonic shock was performed at room temperature to ensure complete reaction and dissolution of quercetin in the solutions. The mixture was centrifuged at 12,000 rpm for 10 min. Then, the supernatant was collected and the color of each supernatant was recorded. The absorbance of each supernatant at 373 nm was measured by UV spectrophotometer, followed by calculation of the quercetin content in each group.

2.5. Preparation of the quercetin-loaded GP (GPQ) hydrogel

To prepare the GPQ hydrogel, 100 mg of GP was dissolved in 1 mL of PBS solution at room temperature, followed by adding 400 μg of quercetin and 5 mg of Irgacure 2959. After quercetin and Irgacure 2959 were completely dissolved, and the mixture was crosslinked under ultraviolet light (30 W, 365 nm) for 2 min to obtain the GPQ hydrogel. The GP hydrogel was prepared by the same method.

2.6. Rheological testing and injectability

The rheological properties of GPQ hydrogels were measured by the Discovery HR2 Rheological Instrument (TA Instruments, New Castle County, USA). The GPQ hydrogel was placed on the test plate. A frequency sweep model (0.1–100 Hz frequency and 1 % strain at 37 °C) was then performed to obtain the storage modulus (G′) and loss modulus (G″). The injectability of GPQ hydrogel was determined by injection with a 29G needle.

2.7. Microstructure observation and swelling ratio

The prepared GPQ hydrogel was frozen at −80 °C and then freeze-dried to obtain dry hydrogel. Subsequently, the sample was gold-plated for 90 s and imaged using a scanning electron microscope (Hitachi, Tokyo, Japan) with an accelerated voltage of 5 kV. At room temperature, the freeze-dried hydrogel (W_{dry}) was immersed in a PBS solution to monitor the change in weight over time (W_{wet}). The swelling ratio (%) was calculated as follow: Swelling Ratio = $(W_{wet} - W_{dry})/W_{dry} \times 100$ %.

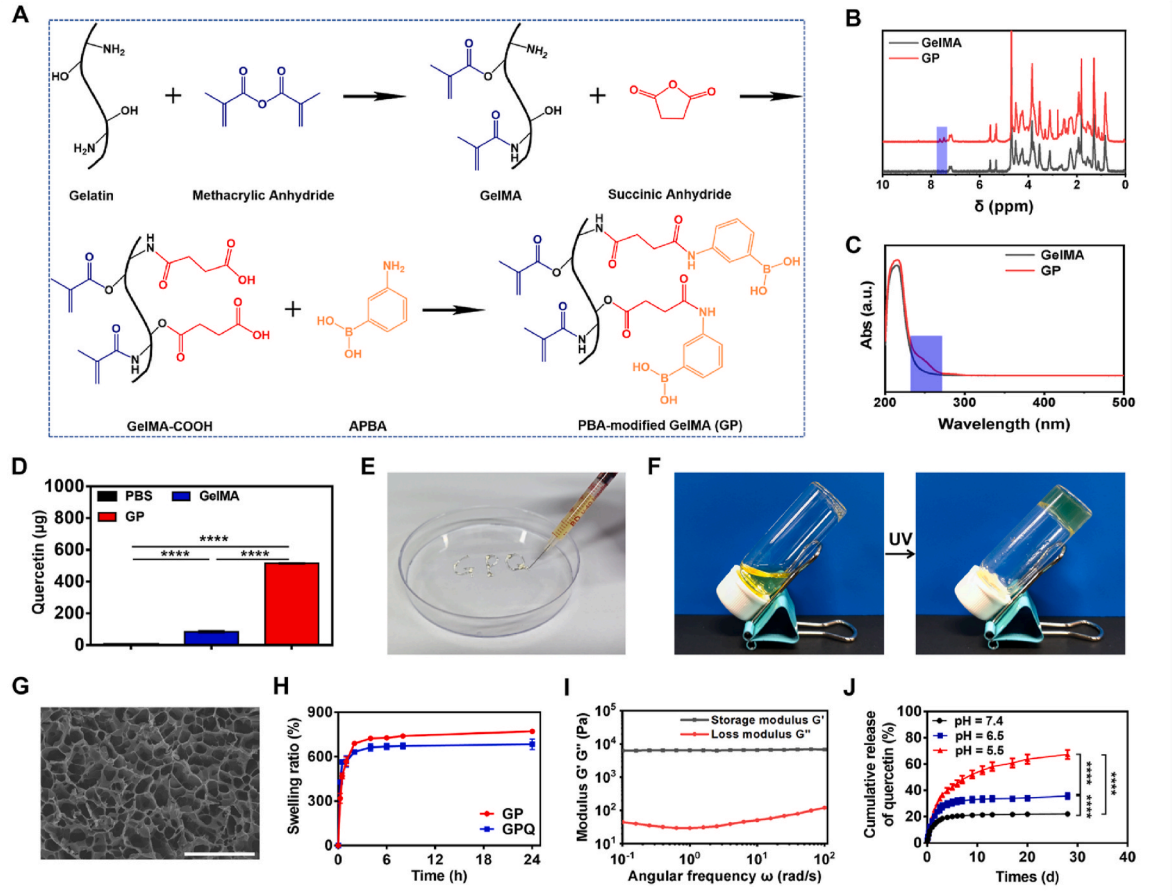

Fig. 1. Synthesis and characterization of the GPQ hydrogels. (A) Synthesis of phenylboronic acid-modified gelatin methacryloyl (GP). (B) ^{1}H NMR and (C) ultraviolet spectra of GelMA and GP. (D) Drug loading of quercetin in PBS, GelMA, and GP solutions (n = 3 per group). (E) Photographs of the injectable GPQ hydrogel. (F) Photographs of the GPQ pregel solution and hydrogel before and after UV crosslinking. (G) Scanning electron microscope image of the GPQ hydrogel (scale bar = 100 μm). (H) Mass swelling curve of the GP and GPQ hydrogels (n = 3 per group). (I) Frequency sweeps rheological analysis of the GPQ hydrogel. (J) Cumulative release curves of quercetin from the GPQ hydrogels under different pH values (pH = 7.4 group: n = 4, pH = 6.5 and pH = 5.5 groups: n = 5). Data represent mean ± SD; ****$p < 0.0001$.

2.8. Responsive release in vitro

The GPQ hydrogels containing 100 μg/mL quercetin were immersed in 10 mL of PBS solution with pH values of 5.5, 6.5, and 7.4, respectively, and then incubated on a shaker at 37 °C and 90 rpm. Subsequently, 1 mL of supernatant was collected at different time points for detection, and an equal volume of PBS solution with different pH values were added to the original solution. The absorbance of each sample at 373 nm was measured by UV spectrophotometer. The quercetin content in each sample was calculated according to quercetin standard curve, and the release curve was established by calculating the cumulative release of quercetin.

2.9. Cell isolation and culture

All animal experiments were approved by the Animal Ethics and Welfare Committee of Southern University of Science and Technology (SUSTech- SL2023030106). Under sterile conditions, the tail NP tissues of Sprague-Dawley (SD) rats (12-week-old, male) were collected and thoroughly rinsed with PBS solution containing 1 % penicillin-streptomycin. They were then transferred to a trypsin-EDTA solution and digested at 37 °C for 30 min. After the termination of digestion, the NP tissues were collected by centrifugation and digested in 0.2 % type II collagenase at 37 °C for 4 h. After removing tissue debris with a 100 μM cell filter, NP cells were collected by centrifugation. The collected cells were re-suspended in a complete medium of DMEM mixed with 10 % fetal bovine serum and 1 % penicillin-streptomycin. They were cultured in a 5 % carbon dioxide and 21 % oxygen incubator at 37 °C, and the medium was changed every 2–3 days. When the cell fusion degree reached 70%–80 %, the cells were passaged for subsequent experiments.

2.10. Biocompatibility

Cytocompatibility was evaluated through cell counting kit-8 assay (CCK-8, C0043, Beyotime, Shanghai, China) and live/dead staining experiments. The NP cells were implanted onto 96-well plates at a density of 5000 cells per well. Complete medium containing different concentrations of GPQ pre-gel (calculated as quercetin concentration) was co-cultured with NP cells for 1, 3, and 5 days. Complete medium without pre-gel served as control group. At the experimental time point, the NP cells were incubated with 100 μL of complete medium containing 10 % CCK-8 working solution for 1 h, and the optical density (OD) value of each well at 450 nm was measured by enzyme-linked immunoassay. The activity of NP cells was observed by live/dead staining on days 1, 3, and 5. The NP cells were stained with calcein-acetoxymethyl ester (calcein-AM) and propidium iodide (PI) for 20 min, and then observed with fluorescence microscope (Leica, Solms, Germany).

Six 12-week-old male SD rats were selected for a subcutaneous implantation study to evaluate the biocompatibility of the GPQ hydrogel in vivo. After continuous inhalation of isoflurane to anesthetize the rats, the back hair was shaved, the back was disinfected with iodophor, and the back skin was cut with a scalpel. The skin and muscle were slowly

separated, and the GPQ hydrogel was implanted (approximately 10 mm in diameter and 2 mm in height). The skin incision on the back was sutured and disinfected with iodophor. Carprofen (5 mg/kg) was administered via subcutaneous injection before surgery and at 12, 24, and 36 h after surgery to alleviate pain in rats. The blood samples were collected from the rats at various time points following subcutaneous implantation of hydrogel for blood routine and blood biochemical tests. The rats were euthanized at a designated time. The hydrogel and surrounding tissues were collected, fixed with paraformaldehyde, and then stained with hematoxylin and eosin (H&E) to assess the degradation of the gel and the regeneration of the surrounding tissues. Some vital organs of the rats were also collected for H&E staining to further assess the effects of the GPQ hydrogel on vital organs.

2.11. Establishment of senescence model of NP cells

The cellular oxidative stress senescence model was constructed with the passage 2 cells. The GPQ pre-gel was diluted to 10 μM with complete medium, and the GP pre-gel was diluted in the same proportion. The stock solution of H_2O_2 was then diluted to 100 μM using complete medium, aforementioned GPQ medium, and aforementioned GP medium, respectively. At this point, complete medium (NC group), H_2O_2 medium (H_2O_2 group), GP + H_2O_2 medium (GP + H_2O_2 group) and GPQ + H_2O_2 medium (GPQ + H_2O_2 group) were obtained. When the density of the cells reached 70 %, the cells were cultured with the above medium for 24 h. Subsequently, the culture was terminated and samples were collected for follow-up experiments.

In the replicative senescence model, the passage 2 cells were selected as the young group and the cells after passage 6 were chosen as the aging group. When the density of the aging cells reached 50 %, the GP and GPQ media mentioned above (labeled Aging + GP group and Aging + GPQ group, respectively) were added, and the samples were collected after 3 days of co-culture with cell density about 90 % for subsequent experiments.

2.12. Senescence-associated β-galactosidase staining

Senescence-associated β-galactosidase (SA-β-Gal) staining (C0602, Beyotime, Shanghai, China) was performed according to manufacturer's instructions. In brief, the NP cells were washed with PBS solution, fixed with SA-β-Gal fixative at room temperature for 15 min, and then incubated with SA-β-Gal working solution at 37 °C without CO_2 overnight. After removing the working solution, three random fields of each group were imaged under an optical microscope and the proportion of β-Gal + cells were calculated using image J software (version: 1.52n, author: Wayne Rasband).

2.13. Immunofluorescence staining

At the designated time point, the cells were washed with PBS solution, fixed with 4 % paraformaldehyde for 15 min, followed by infiltration with 0.5 % Triton X-100 for 10 min. After being blocked with 5 % bovine serum albumin for 1 h, the samples were incubated with a primary antibody overnight at 4 °C (anti-aggrecan: 13880-1-AP, Proteintech, Wuhan, China, 1:400, 1.25 μg/mL; anti-Collagen Type II: 28459-1-AP, Proteintech, Wuhan China 1:300, 1.67 μg/mL; anti-IL-1β: Abcam, ab283818, Cambridge, UK, 1:100, 5.3 μg/mL). After the primary antibody was removed, the samples were incubated with fluorescently conjugated secondary antibody in the dark at room temperature for 1 h. The cell nucleus was stained with Hoechst (Beyotime, Shanghai, China) for 5 min. Then, the samples were washed with PBS solution to remove unincorporated dyes. Images were obtained under a confocal laser scanning microscope (CLSM, ZEISS, Oberkochen, Germany).

2.14. Real-time quantitative reverse transcription PCR (qPCR)

The total RNA of samples was extracted according to the instructions of the FastPure Cell Total RNA Isolation Kit V2 (Vazyme, Nanjing, China). The RNA was then reverse-transcribed into cDNA according to the instructions of the Strand cDNA Synthesis Kit (Vazyme, Nanjing, China). The qPCR analysis was performed in a Quant Studio 5 Flex System (Thermo Fisher Scientific, Waltham, USA) with SYBR qPCR SuperMix Plus (Novoprotein, Shanghai, China). The PCR reaction system for each sample was prepared as follows: 10 μL of SYBR qPCR SuperMix Plus, 0.6 μL of forward primers (10 μmol/L), 0.6 μL of reverse primers (10 μmol/L), 0.4 μL of cDNA template (50 μg/mL), 0.4 μL of ROX II, and 8 μL of RNase Free Water. The subsequent reaction is then conducted using a two-step approach, as follows. Step 1: 95 °C for 1 min; step 2: 95 °C for 20 s, 60 °C for 1 min, and 40 cycles, annealing temperature: 60 °C. β-actin was used as the housekeeping gene, and the relative expression level (compared with the NC group and young group) of target gene was calculated using the $2^{-\Delta\Delta\ ct}$ method. All the experiments were performed on three separate occasions. The sequences of the primers used are listed in Supplementary Table 1.

2.15. Establishment of IVDD model in rats

All animal experiments have been approved by the Animal Ethics and Welfare Committee of Southern University of Science and Technology (SUSTech- SL2023030106). In this study, ten male SD rats aged 10–12 weeks were selected as young rats and purchased from Guangdong Medical Laboratory Animal Center. Five male SD rats aged 20 months were selected as old rats and purchased from Jiangsu Wukong Biotechnology Co. LTD. In order to minimize the influence of individual differences on the experiment, experimental groups were set up in different intervertebral disc segments of the same rat. The model of IVDD in rats was established by a needle puncture method as described in previous researches [33,34]. After continuous inhalation of isoflurane anesthesia, the tail skin was disinfected with iodophor, the location of the tail disc segment was determined, and the tail skin was cut open with a scalpel. Then, 20G needle was punctured in the center of C5-10 IVD, rotated axially for 360°, and held for 30 s to establish the IVDD model. Subsequently, 5 μL of GPQ pregel solution with different concentrations, GP pregel solution, and PBS solution were injected into IVDD model with microinjector, respectively. To reduce secondary damage caused by treatment, the sample was injected through the same needle path within the IVD gap. The samples were irradiated with ultraviolet light for 30 s. As the sham group, C4-5 IVD was only exposed without being punctured. Finally, the incision was sutured and disinfected with iodophor. Carprofen (5 mg/kg) was administered via subcutaneous injection before surgery and at 12, 24, and 36 h after surgery to alleviate pain in rats. Five rats in each group were killed at each experimental time point for radiological and histological evaluation.

2.16. Evaluation of treatment efficacy for IVDD

In vivo experimental results were evaluated by radiology and histology. Firstly, at different predetermined postoperative time points, magnetic resonance imaging (MRI, GSMED, Shenzhen, China) scans were performed on each group of rats under anesthesia. The gray value of NP tissue in MRI t2-weighted images was measured by ImageJ software (version: 1.52n, author: Wayne Rasband) to reflect the water content of NP tissue. At the same time, the Pfirrmann grade was used to evaluate the degree of IVDD in each group [35]. Then, the rats were euthanized, and the tail tissues were isolated and fixed with 4 % paraformaldehyde. Micro-CT imaging system (Bruker, Billerica, USA) was used to scan the tail tissues with the voxel size of 20.4 μm and resolution of 1344 × 2016, and the sagittal plane images were obtained after reconstruction. Disc height index (DHI) was measured and calculated using ImageJ software as a previous study described [36], with the

calculation method shown in Fig. S1.

All samples were fixed in 4 % paraformaldehyde for 2 days and decalcified in EDTA decalcified solution for 4 weeks. Then, the samples were rinsed with water overnight, dehydrated with gradient alcohol, and then clarified with xylene. After embedding and slicing, hematoxylin-eosin (H&E) and saffron red-O/fast green (SF) staining were performed. Histological grading of IVD in rats was performed according to the methods of previous studies [37], as shown in Table S2. The expressions of p21 (GB11153, Servicebio, Wuhan, China, 1:50, 6.00 μg/mL) and Col II (GB11021, Servicebio, Wuhan, China, 1:200, 2.50 μg/mL) were detected by immunohistochemical staining.

2.17. Establishment of LBP model in rats and behavioral studies

The anterior lumbar puncture model of rats was used to mimic the LBP caused by IVDD. Seventeen male SD rats aged 10–12 weeks were divided into the sham, GPQ, and PBS groups (five rats in the sham group, six rats in the GPQ group and six rats in the PBS group). After continuous inhalation of isoflurane, the Lumbar 4–5 (L4-5) IVD levels were located by bilateral iliac ridge lines. After shaving the abdominal hair, the skin was disinfected and cut open to expose the enterocoelia, and the viscera of the rat were retracted to expose the L4-5 IVD levels. A 20G sterile needle was punctured vertically into the IVD, rotated axially for 360°, and hold for 30 s. The GPQ group and PBS group were treated with the injection method mentioned above. The procedures of disc exposure, needle puncture, and treatment were performed by three experimenters in double-blind conditions. Carprofen (5 mg/kg) was administered via subcutaneous injection before surgery and at 12, 24, and 36 h after surgery to alleviate pain in rats. Behavioral observations of rats, including the sensitivity of deep lumbar axial tissues to noxious mechanical force, the sensitivity of the lower extremities to harmless mechanical pain stimuli, and response of the plantar skin to heat damage stimulation, were performed before and 8 weeks (once a week) after surgery.

The sensitivity of deep lumbar axial tissues to noxious mechanical force was measured using a pressure algometer (Bioseb, Vitrolles, France) as described in previous research [38]. In brief, mechanical force was applied at a speed of approximately 100 g/s to the back at the L4-5 IVD levels of the lumbar spine to evaluate pressure algometry thresholds (PATs) that caused audible vocalizations or discomfort.

The sensitivity of the lower extremities to harmless mechanical pain stimuli was measured by the von Frey test. The rats were placed alone in cages with metal mesh at the bottom and acclimated for 15 min. A set of calibrated von Frey filaments (Stoelting, Wood Dale, USA) were applied to the sole of the hind paw from below. The test started at 2.0 g, applying enough pressure to induce filament bending and then maintaining it for 6 s. The intensity of stimulation was escalated if there was no response from the rats. If foot retraction reflex occurred, reduced the stimulation and repeated the previous intensity.

The response of rat plantar skin to heat damage stimulation was examined by Hargreaves test. The rats were placed alone in a cage with a transparent glass panel at the bottom and acclimated for 15 min. The movable thermal radiation source was focused on the sole of the rat through the glass plate, and the latency period of the rat response was recorded. All tests were performed 3 times for each rat, with an interval of at least 5 min, and the measurement results were recorded. When the rats reacted, the heat source was turned off. To prevent tissue damage, the heat source was automatically turned off after 20 s.

All tests were performed 3 times for each rat, with an interval of at least 5 min, and the measurement results were recorded.

After 8 weeks, all samples were collected and fixed in 4 % paraformaldehyde for 2 days and decalcified in EDTA decalcified solution for 4 weeks. Then, the samples were rinsed with water overnight, dehydrated with gradient alcohol, and then clarified with xylene. After embedding and slicing, immunofluorescence staining of nerve growth factor (NGF, GB111206, Servicebio, Wuhan, China, 1:300, 3.57 μg/mL) was performed. Then the proportion of NGF positive cells in NP tissues were calculated using image J software (version: 1.52n, author: Wayne Rasband).

2.18. Statistical analysis

Statistical analysis was performed with GraphPad Prism 9.0 software (San Diego, USA). Shapiro-Wilk test was used to check whether the data conforms to the normal distribution. Data consistent with normal distribution are shown as mean ± SD. Statistical analysis was performed using a two-tailed Student's *t*-test or one-way ANOVA with Tukey's multiple comparisons. Data that does not conform to normal distribution was performed using Kruskal-Wallis test. Statistical significance was defined as $^{*}p < 0.05$, $^{**}p < 0.01$, $^{***}p < 0.001$ and $^{****}p < 0.0001$.

3. Results

3.1. Synthesis and characterization of the GPQ hydrogel

The GP material was synthesized by grafting double bonds and PBA groups onto gelatin molecular chains through a three-step chemical reaction. A schematic diagram was shown in Fig. 1A. The ^{1}H NMR spectra in Fig. 1B revealed that new characteristic proton peaks corresponding to the benzene rings in GP appeared in the range of 7.3–7.7 ppm, suggesting the successful grafting of PBA groups onto GelMA. The same result was obtained through UV spectroscopy analysis. Due to the introduction of PBA groups, the UV absorption of GP increased at 230–270 nm (Fig. 1C). Under normal or alkaline conditions, the o-phenol group in quercetin can form a borate ester bond with the boric acid group in PBA (Fig. S2), which may improve the solubility of quercetin in aqueous solutions. Quercetin is a yellow powder, and its concentration directly correlates with the intensity of the solution's color. After sufficient reaction with quercetin, the GP solution presented a more yellow color than the PBS and GelMA solutions (Fig. S3). We then calculated the calibration curve of quercetin using a UV–vis spectrophotometer to assess the content of quercetin dissolved in the GP solution (Figs. S4 and S5). As shown in Fig. 1D, the solubility of quercetin was significantly greater in the GP solution than in the PBS and GelMA solutions, achieving 515.3 ± 5.4 μg/mL. The GPQ pregel solution was injected easily through a needle with an outer diameter of 0.33 mm (Fig. 1E). We added 400 μg of quercetin to a 10 % w/v GP solution in order to fully dissolve the quercetin. After adding Irgacure 2959, a photoinitiator that can initiate polymerization at a concentration of 0.1–1% w/v, the GPQ pregel solution could be exposed to UV illumination for 2 min to obtain a yellow GPQ hydrogel (Fig. 1F). As observed by scanning electron microscopy (SEM), the GPQ hydrogel exhibited thin-walled interconnected porous structures with pore diameters of approximately 20–50 μm (Fig. 1G). Rheological analysis revealed that the storage modulus G′ of the GPQ hydrogel was approximately 6500 Pa, and the loss modulus G″ was approximately 40–100 Pa in the scanning frequency range of 0.1–100 rad/s (Fig. 1I). However, the addition of quercetin did not significantly change the swelling rate of the hydrogel, which still reached 684.9 ± 35.4 % after immersion in PBS solution for 24 h, indicating good water absorption by the hydrogel (Fig. 1H). Finally, we examined the drug release curves of quercetin from GPQ hydrogels in PBS solutions at different pH values. After 30 days of measurement, it was found that the lower the solution pH, the faster the drug release rate (Fig. 1J). Overall, we successfully synthesized GP that could significantly increase the drug loading capacity of quercetin. The prepared GPQ hydrogel was photocrosslinkable, injectable, and capable of responsive release of therapeutic drugs in the acidic microenvironment, which may be suitable for treatment of closed tissues such as the IVD.

3.2. Biocompatibility of the GPQ hydrogel

The effect of the GPQ hydrogel on the proliferation and viability of NP cells was verified by CCK-8 assay and live/dead cell staining. On the first day, there was no significant difference between the GPQ group and the control group. On the third and fifth days, the 10 μM group exhibited the greatest increase in proliferation. However, the OD values of the 50 μM and 100 μM groups decreased relative to that of the control group. On the fifth day, the OD values of the 50 μM group still reached more than 85 % of the control group, while the 100 μM group only 58 % of the control group (Fig. S6A). The same trend was observed in the live/dead staining results, and it was encouraging that there were almost no dead cells in any of the groups (Fig. S6B). In conclusion, the GPQ hydrogels exhibited good biocompatibility in vitro, and when the concentration was less than 50 μM, there was no obvious inhibition of cell proliferation. Considering that the optimal proliferative activity was demonstrated by the 10 μM concentration, we chose 10 μM for functional verification at the cellular level.

Then, we evaluated the biocompatibility of the GPQ hydrogels in vivo by a subcutaneous implantation test. H&E staining revealed mild granulocyte and macrophages infiltration around the hydrogel at 2 weeks after implantation. As time increased, by the fourth week, the hydrogel was further degraded and gradually replaced by newly grown blood vessels and tissues, with a marked decrease in its surrounding macrophages and only a few granulocytes remaining. (Fig. S6C). To further monitor the overall health of animals during the hydrogel implanted period of 4 weeks, the blood routine and blood biochemical tests were performed at different time points. As showed in Figs. S7A and B, the blood routine and blood biochemistry results were within normal values range at 7, 14, and 28 days of subcutaneous implantation, indicating no systemic toxicity of the degradation byproducts. H&E staining of vital organs further confirmed this conclusion (Fig. S7C). These results indicated that the GPQ hydrogels exhibited good biocompatibility in vivo.

3.3. The GPQ hydrogel alleviated senescence caused by oxidative stress

Oxidative stress is the most common trigger of cellular senescence and is closely related to the progression of IVDD. Therefore, we performed previous studies and used hydrogen peroxide to simulate oxidative stress injury in NP cells in vitro [39]. Then, the injured NP cells were incubated with the GP or GPQ hydrogels to evaluate the effect of oxidative stress on cellular senescence. SA-β-gal activity is an important biomarker for evaluating cell senescence, and its activity increases in

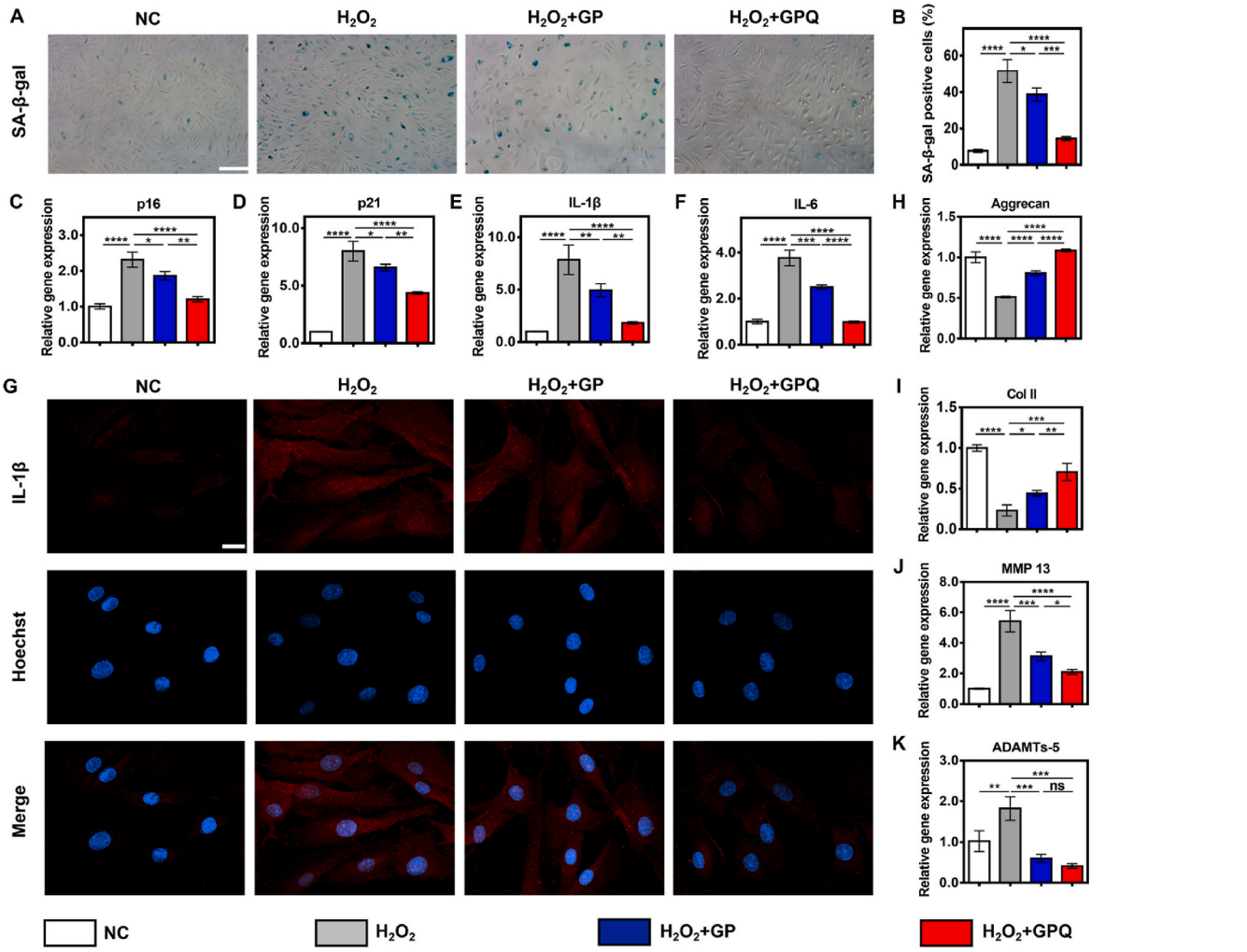

Fig. 2. The GPQ hydrogel alleviated NP cells senescence caused by oxidative stress. (A) SA-β-gal staining of NP cells in different groups (scale bar = 100 μm). (B) Semi-quantitative analysis of SA-β-gal positive cells in different groups. (C–F) The mRNA expression levels of p16, p21, IL-1β, and IL-6 in different groups of NP cells. (G) Confocal images of IL-1β immunofluorescence for each group (scale bar = 20 μm). (H–K) The mRNA expression levels of aggrecan, Col II, MMP 13, and ADAMTs-5 in different groups of NP cells. Data represent mean ± SD; n = 3 per group; statistical significance was analyzed by one-way ANOVA; *$p < 0.05$, **$p < 0.01$, ***$p < 0.001$, and ****$p < 0.0001$, ns: no significance.

senescent cells [40]. SA-β-gal staining revealed that the number of positive cells increased approximately 6-fold in the H_2O_2 group, whereas the number of positive cells decreased in the H_2O_2+GP and H_2O_2+GPQ groups. In particular, in the GPQ group, the expression level decreased to only 1.8-fold that in the NC group (Fig. 2A and B). p16 and p21 are two classical cellular senescence-related genes that are highly expressed in senescent cells [40]. The expression of these two markers was detected at both the gene and protein levels. The results demonstrated a 1.3-fold and 7-fold increase in the expression of these genes (Fig. 2C and D), as well as a respective 1.2-fold and 2.1-fold increase in protein levels (Figs. S8A–C) in the H_2O_2 group compared to the NC group. However, in the H_2O_2+GPQ group, the expression of both senescence genes decreased to only half of the level in the H_2O_2 group, while protein levels reduced to approximately 0.60 and 0.64 times those of the H_2O_2 group. In addition, we examined the changes in the expression of IL-1β and IL-6, two typical proinflammatory factors of the SASP, to comprehensively evaluate the effect of the GPQ hydrogels on cell senescence. As shown in Fig. 2E and F, the expression levels of both were elevated after H_2O_2 treatment (IL-1β: ~7.8-fold; IL-6: ~3.8-fold), and the inhibitory effect of GPQ on both inflammatory factors was more prominent, demonstrating comparable levels to those of the NC group. The same trend was also observed in the immunofluorescence experiments, in which the IL-1β fluorescence intensity increased in the H_2O_2 group, while the fluorescence intensity in the H_2O_2+GPQ group was close to that in the NC group (Fig. 2G). In addition, we examined the level of IL-6 secreted by cells in the culture medium by enzyme-linked immunosorbent assay (ELISA), which decreased to about 70 % of that in the H_2O_2 group after treatment with GPQ hydrogel (Fig. S8F).

Cell senescence and the SASP lead to metabolic disequilibrium, and the loss of bound water molecules due to degradation of the ECM is another major characteristic of IVDD. The ECM of the NP tissue is mainly composed of aggrecan and Col II. qPCR revealed a significant reduction in the expression of aggrecan and Col II (decrease to ~0.51-fold and ~0.23-fold respectively) in NP cells after H_2O_2 treatment, indicating that the capacity for ECM synthesis in NP cells significantly decreased under oxidative stress conditions. In the H_2O_2+GP and H_2O_2+GPQ groups, the expression of aggrecan and Col II exhibited opposite trends, indicating that the hydrogels could maintain ECM synthesis (Fig. 2H and I). Immunofluorescence experiments also confirmed this result, with aggrecan and Col II fluorescence intensity diminished in the H_2O_2 group, while the fluorescence intensity of the H_2O_2+GPQ group was close to that of the NC group (Figs. S9 and S10). Moreover, the expression of catabolic related indicators MMP13 and ADAMTs-5 was measured at gene and protein levels. The expression of MMP13 and ADAMTs-5 increased in the H_2O_2 group, but decreased in the H_2O_2+GP and H_2O_2+GPQ groups, suggesting that the hydrogels effectively inhibited

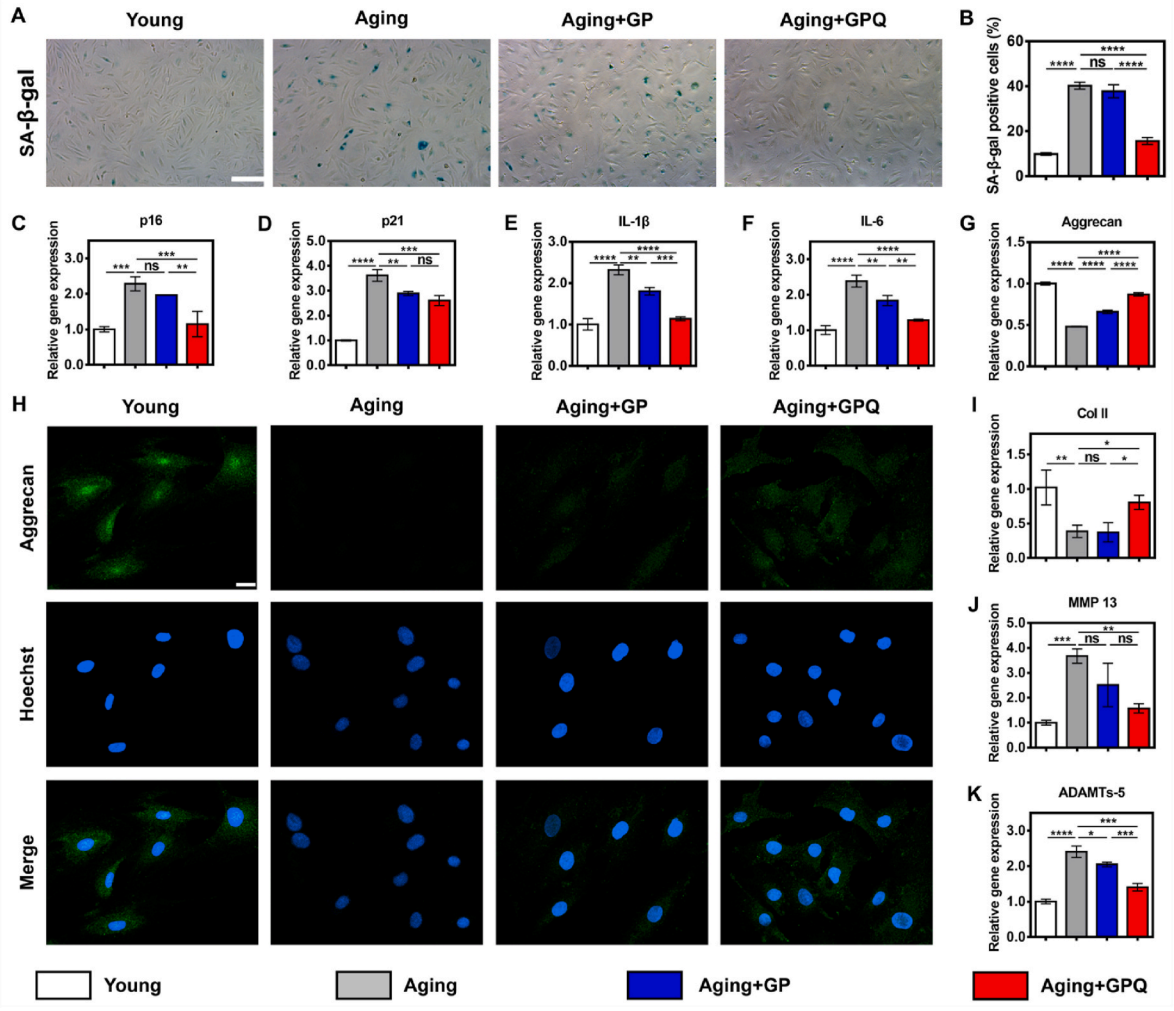

Fig. 3. The GPQ hydrogel alleviated NP cells replicative senescence. (A) SA-β-gal staining of NP cells in different groups. (scale bar = 100 μm) (B) Semi-quantitative analysis of SA-β-gal positive cells in different groups. (C–F) The mRNA expression levels of p16, p21, IL-1β, and IL-6 in different groups of NP cells. (G–H) The mRNA expression levels of aggrecan and confocal images of aggrecan immunofluorescence of NP cells in each group. (scale bar = 20 μm) (I–K) The mRNA expression levels of Col II, MMP 13, and ADAMTs-5 in different groups of NP cells. Data represent mean ± SD; n = 3 per group; statistical significance was analyzed by one-way ANOVA; $^{*}p < 0.05$, $^{**}p < 0.01$, $^{***}p < 0.001$, and $^{****}p < 0.0001$, ns: no significance.

catabolism induced by oxidative stress (Fig. 2J and K; Figs. S8A, D, E). Taken together, these findings showed that the GPQ hydrogel was able to reduce the number of senescent cells and the expression of inflammatory factors, as well as restore the metabolic balance of cells.

3.4. The GPQ hydrogel improved cellular replicative senescence

Replicative senescence is another common cause of cellular senescence and is closely associated with age-related diseases. Previous studies have shown that replicative senescence occurs in NP cells after six passage of culture [41]. Therefore, we used passage 2 NP cells as the young group and the cells after passage 6 as the aging group to evaluate the effect of the GPQ hydrogel on replicative cell senescence. SA-β-gal staining revealed that the number of positive cells increased in the aging group to approximately 4.0 times that in the young group. The GP hydrogel did not reduce the activity of SA-β-gal in the aging cells, while the number of positive cells decreased significantly in the aging + GPQ group and was only 1.5 times greater than that in the young group (Fig. 3A and B). The expression of the two senescence-related genes p16 and p21 increased by 1.3-fold and 2.6-fold, respectively, in the aging group (Fig. 3C and D). The difference was not significant in the aging + GP group; moreover, the expression of these two genes in the aging + GPQ group was only 0.5-fold and 0.7-fold of that in the aging group. The levels of p16 and p21 proteins in the aging group were 1.8 and 2.6 times higher than those in the young group, whereas after treatment with GPQ hydrogel, the two proteins decreased to only 0.5 and 0.7 times of those in the aging group, respectively (Fig. S11 A-C). The levels of IL-1β and IL-6, two representative SASP factors, in the aging group were 2.3 and 2.4 times greater than those in the young group, respectively (Fig. 3E and F). After treatment with the hydrogels, the expression of IL-1β and IL-6 decreased, especially in the aging + GPQ group, whose expression was more similar to that of the young group. A similar trend was observed in the immunofluorescence results for IL-1β, with significantly higher fluorescence intensity in the aging group and much weaker in the aging + GPQ group (Fig. S12). The levels of IL-6 secreted by the cells were also quantified, and the ELISA results revealed that treatment with GPQ hydrogel led to a significantly reduced concentration of secreted IL-6 compared to the aging group (Fig. S11F). In replicative senescent cells, cellular metabolism is also altered. As shown in Fig. 3G and I, compared with those in the young group, the expression of aggrecan and Col II in the aging group decreased by 54 % and 61 %, respectively. The synthesis of ECM in the hydrogel groups could be restored to a certain extent; in particular, the aging + GPQ group recovered to 81 % and 89 % of the young group, respectively. Aggrecan and Col II immunofluorescence also exhibited the same trend, with almost no green fluorescence in the aging group, while the fluorescence intensity in the GPQ group was similar to the young group (Fig. 3H, Fig. S13). In addition, the qPCR results for catabolic indices also supported the same conclusion (Fig. 3J and K). The expression of MMP13 and ADAMTs-5 genes in the aging group was 3.7 and 2.4 times greater than that in the young group, respectively. But the expression of the two catabolism-related genes in the aging + GPQ group decreased to 0.4 and 0.6 times of that in aging group, respectively. The levels of both proteins in the aging group were 1.7 and 1.5 times higher than those in the young group, and both decreased to about 0.7 times of those in the aging group after treatment with GPQ hydrogel (Figs. S11A, D, E). These results indicated that the GPQ hydrogel could reduce the number of replicative senescent cells, alleviate metabolic imbalances, and promote functional recovery.

3.5. Local injection of the GPQ hydrogel attenuated IVDD in rats

Previous studies have shown that the expression of age-related biomarkers in IVDs is increased in a puncture-induced IVDD model [42,43]. To investigate the effect of the GPQ hydrogel on IVDD treatment, we injected the GPQ hydrogel, GP hydrogel, or PBS solution into the damaged IVD tissues of a puncture-induced IVDD model in rats, and set a concentration gradient in the GPQ group to assess the efficacy at 4 and 8 weeks (Fig. 4A). Radiography is a reliable indicator of IVD degeneration and repair and is also an important reference for the clinical diagnosis of spinal degenerative diseases. We calculated the disc DHI of each group by micro-CT images, and the results showed that the DHI of the PBS group decreased to only 51.8 % of that of the sham group at 4 weeks. The disc height was maintained in the GPQ and GP groups to a certain extent. Although there was no significant difference in different concentration of the GPQ groups, the 50 μM GPQ group was 1.2 times greater than that in the GP group and 1.6 times greater than that in the PBS group, showing the closet level to the sham group (Fig. 4B and F). MRI T2-weighted intensity can reflect the water content of NP tissue, and a stronger signal represents a greater water content. As shown in Fig. 4C and G, the signal intensity in the PBS group decreased to 45.5 % of that in the sham group. Compared with those in the PBS group, the signals in both the GPQ and GP groups were more intense at 4 weeks, but the difference was not significant. The Piffrmann grade is the most widely used method for evaluating the severity of IVDD in the clinic, with grades I to V indicating an aggravated degree of degeneration [35]. By summarizing the MRI images of each group, we found that at 4 weeks, the disc structure of the sham group was complete, all of which were grade I, while severe degeneration occurred in the PBS group, which was mainly grade IV. The grade of degeneration was reduced in the treatment group, with grade III predominating in the GP group and grade II predominating in the GPQ groups, besides grade I discs still presented in the 50 μM and 10 μM GPQ groups (Fig. 4H). At 8 weeks, the DHI of the PBS group further decreased to 45.3 % of that of the sham group. A reduction in disc height was delayed in the GPQ and GP groups. Although there was no significant difference in different concentration of the GPQ groups, the 50 μM and 10 μM GPQ groups exhibited significantly greater therapeutic effects compared with GP group (Fig. 4D and I). MRI images revealed that the signal intensity in the PBS group decreased to 19.7 % of that in the sham group at 8 weeks, and the Piffrmann grades were predominate with V, indicating severe degeneration (Fig. 4E, J, and K). The signal intensity in the GP group was 2.6 times greater than that in the PBS group, but the Piffrmann grade decreased to mainly level IV. The GPQ groups exhibited significantly greater signal strength than both the GP and PBS groups, but the Piffrmann grade was also lower than that at 4 weeks, with grades II and III being predominant (Fig. 4E, J, and K).

H&E and SF staining revealed that the NP tissues in the PBS group were atrophied at 4 weeks, and the AF layer structure was disrupted; however, distinguishable AF and NP boundaries were still observed (Fig. 5A and B). At 8 weeks, the degeneration worsened, and the normal structure of the IVD was no longer recognizable; the IVD was replaced by disorganized tissue with no clear boundaries (Fig. 5E and F). The GP treatment alleviated this degeneration trend, but compared with those in the sham and GPQ groups, the NP tissue in the GP group was reduced, and AF defects were obvious. The GPQ groups exhibited relatively complete retention of the IVD structure. Compared with those in the GP and PBS groups, the NP tissue area was larger, presenting a more circular tissue shape, and the boundaries between the AF and NP were clearer (Fig. 5A and B). However, at 8 weeks, there were obvious AF defects in the 10 μM and 2 μM GPQ groups (Fig. 5E and F). The histological score can reflect the results of H&E and SF staining in each group more directly, and a lower score represents a better treatment effect. The histological scores in the GPQ groups were lower than those in the PBS group at 4 weeks, but there was a significant difference only in the 50 μM GPQ groups (Fig. S14A). However, the scores of all groups at 8 weeks were greater than those at 4 weeks, indicating an increase in degeneration (Figs. S14B and C). Compared to the other experimental groups, the 50 μM GPQ groups showed the lower score, demonstrating that this treatment was more effective in delaying IVDD (Fig. S14B). The expression of p21 and Col II was evaluated by immunohistochemistry. Compared with other experimental groups, the 50 μM GPQ group had the lowest expression of p21 and the strongest signal intensity of Col II

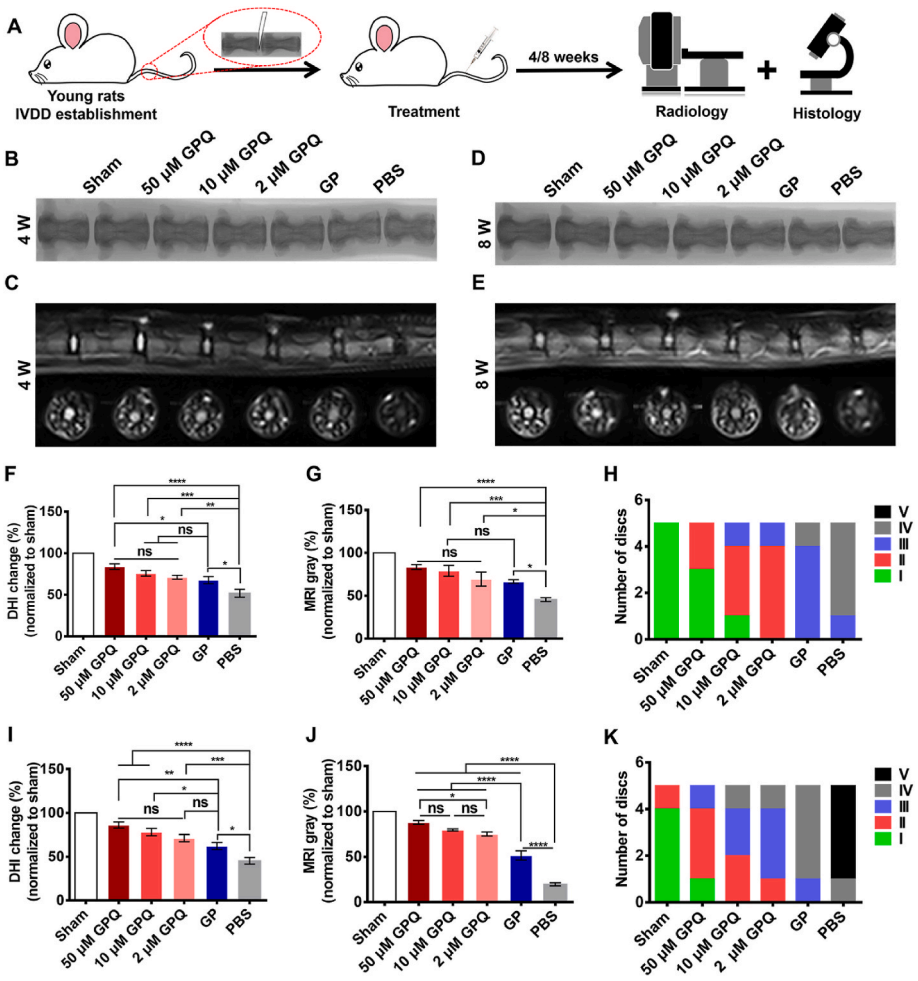

Fig. 4. Radiological evaluation of the GPQ hydrogel in the young rat IVDD model. (A) A schematic diagram illustrating the experimental design. (B) Representative micro-CT images at 4 weeks. (C) Representative T2-weighted MRI sagittal and cross-sectional images at 4 weeks. (D–E) Representative micro-CT and T2-weighted MRI images at 8 weeks. (F–H) Analysis and quantification of (B) and (C). The changes of DHI in each group were calculated by 4 weeks Micro-CT images. (F) Relevant average gray value (G) and Pfirrmann grade (H) analysis of MRI images at 4 weeks. (I–K) Quantification and analysis of radiological results at 8 weeks. Data represent mean ± SD; n = 5 per group; statistical significance was analyzed by one-way ANOVA; $*p < 0.05$, $**p < 0.01$, $***p < 0.001$, and $****p < 0.0001$, ns: no significance.

(Fig. 5C, D, G, H, and Fig. S14D-G).

Combining the imaging and histological findings, it was observed that in the rat IVDD model, the GPQ hydrogel effectively delayed the progression of IVDD. However, the difference among the GPQ groups of various concentrations was not obvious in the imaging results, the high-concentration group exhibited a significant advantage at the histological level.

3.6. A high concentration of the GPQ hydrogel improved IVDD in aged rats

Increasing age leads to the deterioration of body function, increasing the difficulty of treating degenerative diseases in elderly people. Considering that IVDD is closely related to age, we further evaluated the efficacy of the GPQ hydrogel for 8 weeks in 20-month-old rats (Fig. 6A). The micro-CT results revealed that disc height was restored in both the GPQ and GP groups, but the difference between these groups was not significant, and only the 50 μM GPQ group exhibited a mild improvement (Fig. 6B and D). The quantitative analysis of signal intensity in T2-weighted MRI images (Fig. 6C and E) showed that there was no difference in signal intensity among the 10 μM GPQ, 2 μM GPQ, GP and PBS groups. The results also indicated that in the 10 μM GPQ, 2 μM GPQ and GP groups, although the hydrogel could preserve the height of the IVD, they were difficult to restore the degree of hydration in NP. However, the signal strength in the 50 μM GPQ group was significantly greater than that in the other treatment groups. The Piffrmann scores also showed the same trend, with predominantly grade IV and V discs in the GP and PBS groups, grade III and IV discs in the 10 μM and 2 μM GPQ groups, and grade II discs in the 50 μM GPQ group (Fig. 6C and F). H&E and SF staining revealed that there was almost no NP tissue in the GP or PBS groups, which was replaced by disordered AF-like tissue. In the 10 μM and 2 μM GPQ groups, the NP tissue significantly shrinkage, the AF layered structure was disrupted, and the AF tissue extended into the NP. The 50 μM GPQ group retained relatively intact NP tissue, although the boundaries between the NP and AF became unclear (Fig. 6H and I). The histological scores further confirmed these results (Fig. 6G). The immunohistochemical results for p21 and Col II confirmed that the expression of p21 decreased and that of Col II increased in the 50 μM GPQ group (Figs. S15A–D). In conclusion, the 50 μM GPQ hydrogel could effectively maintain the histological structure of IVDs and improve the progression of IVDD in an aged rat IVDD model.

3.7. The GPQ hydrogel mitigated LBP caused by IVDD

IVDD is the most common pathogenic factor for LBP, and LBP is also the most common clinical symptom of IVDD. Therefore, whether the GPQ hydrogel can alleviate LBP caused by IVDD is also the most concerning problem in clinical treatment. We established an animal model

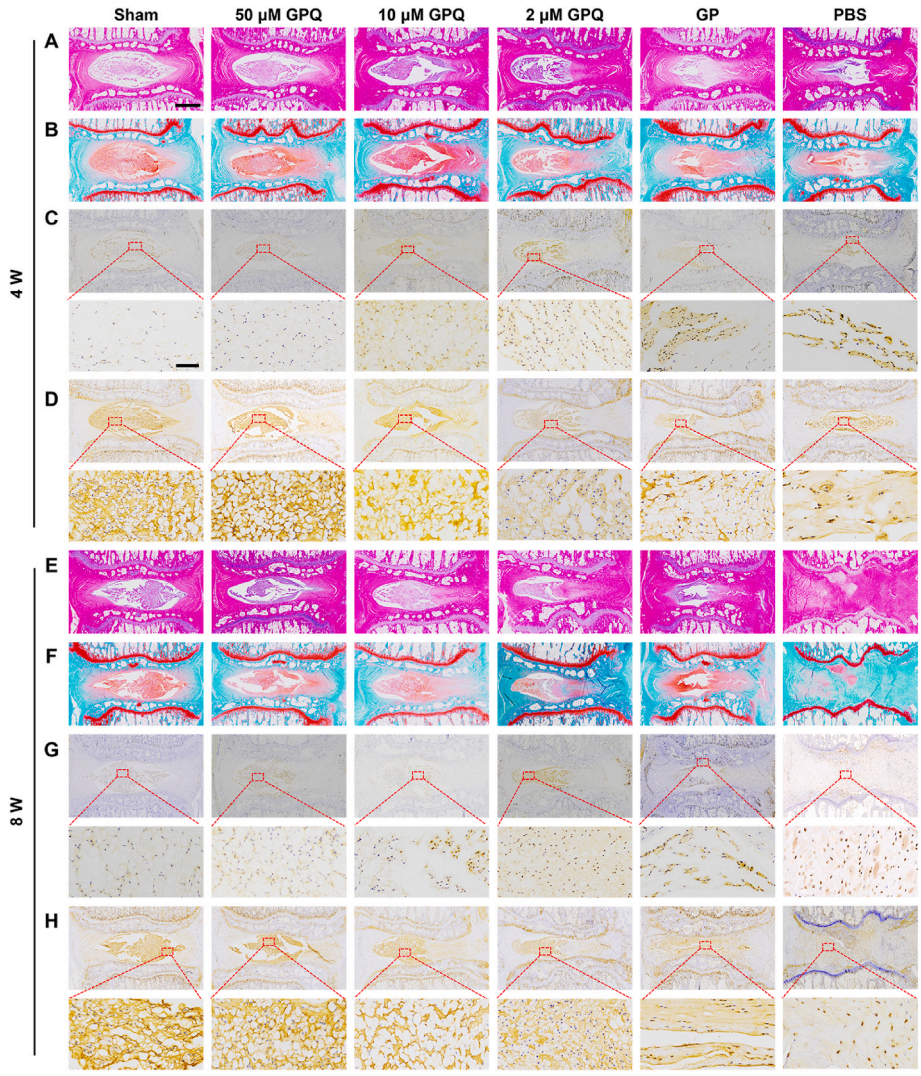

Fig. 5. Histological assessment of the GPQ hydrogel in the young rat IVDD model. The H&E (A), SF (B), p21 (C), and Col II (D) staining of histological results in different groups at 4 weeks. The H&E (E), SF (F), p21 (G), and Col II (H) staining of histological results in different groups at 8 weeks. (scale bar = 1000 μm up, 80 μm below).

of anterior lumbar puncture in young rats to observe pain-related behavioral changes (Fig. 7A). The rats were divided into the Sham, GPQ and PBS groups, and the GPQ group was treated with the 50 μM GPQ hydrogel. MRI results showed that the GPQ hydrogel maintained the degree of hydration of the NP tissue (Fig. 7B). Pressure algometry thresholds (PATs) were used to assess pain sensitivity and threshold levels in response to applied pressure. On Day 0 (before puncture), the baseline levels of PATs in each group were similar, while the PATs levels in the GPQ and PBS groups were significantly lower than those in the Sham group at postoperative weeks 1 and 2, suggesting successful induction of LBP (Fig. 7C). Starting from the third week, the PATs values in the GPQ and PBS groups began to increase, indicating that the injury began to recover. However, the increase in the GPQ group was more rapid than that in the PBS group, with a significant difference at 4 weeks (508.3 ± 10.6 vs. 468.4 ± 18.4). At 8 weeks, the GPQ and PBS groups had stabilized, and the increase in the GPQ group was more significant, reaching 585.4 ± 34.6 (Fig. 7C). These results proved that the GPQ hydrogel could relieve LBP in rats. In addition, mechanical and thermal pain in the lower extremities was measured by the Von Frey and Hargreaves tests. However, the results revealed no significant differences among the three groups, possibly because through anterior puncture, the IVD did not herniate backward or compress the nerve root to cause symptoms in the lower extremity (Fig. 7D and E). During IVDD, nerve endings expand from the outer AF to the NP tissue, accompanied by elevated levels of neurotrophic factors such as NGF, resulting in increased sensitivity to pain. As shown in Fig. 7F and G, the expression of NGF was lower in the IVDs of the GPQ group than that in the PBS group, indicating that nerve growth was reduced after treatment with the GPQ hydrogel. In conclusion, the GPQ hydrogel effectively reduced the sensitivity of the degenerated lumbar IVD to mechanical forces in rats.

4. Discussion

LBP caused by IVDD has always been a major health problem that troubles people's lives, causing enormous economic losses to society and individuals. In recent years, an increasing number of studies have confirmed that the senescence of NP cells plays an important role in the process of IVDD, and treatments targeting senescence can effectively delay IVDD [42,43].

Quercetin is a kind of natural flavonoid that is widely found in edible plants such as fruits, vegetables and tea. It has the characteristics of low cost and wide availability and can play an anti-senescence role in many diseases. Some studies have shown that quercetin can ameliorate the senescence of NP cells and IVDD. However, due to the anatomic

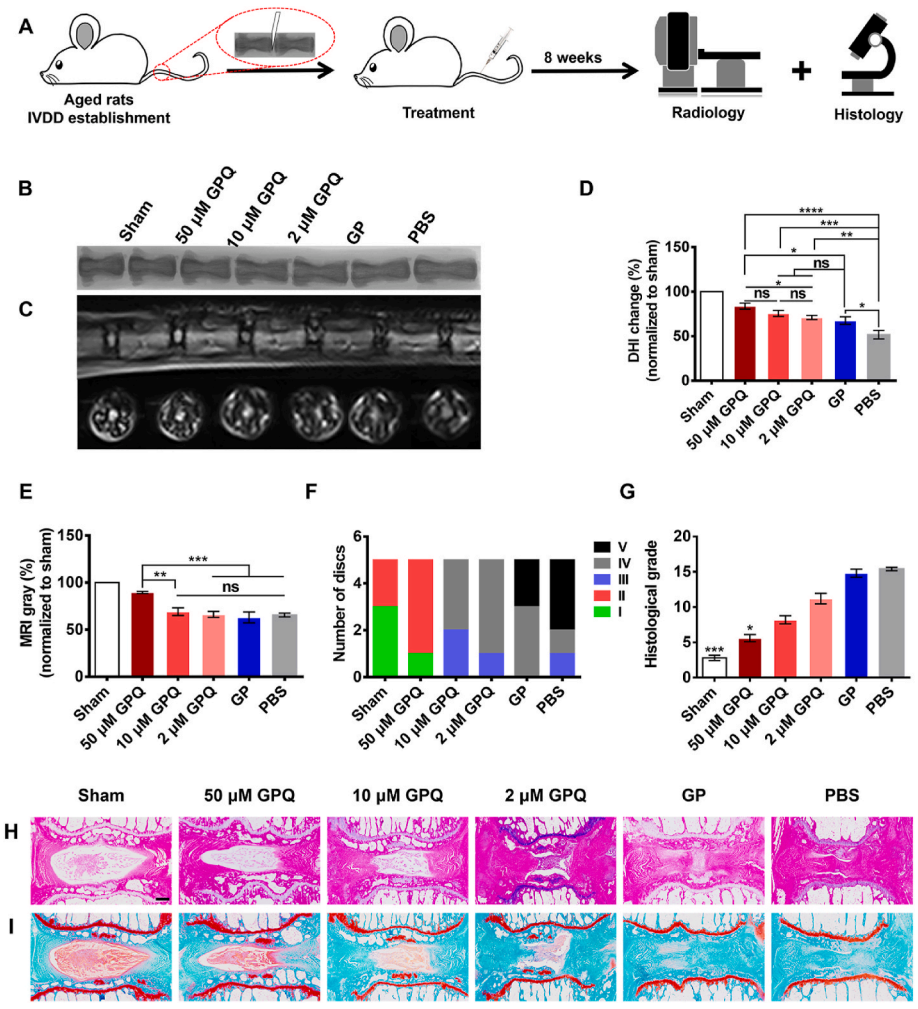

Fig. 6. Radiological and histological assessment of the GPQ hydrogel in the aged rat IVDD model. (A) Schematic illustration showing the overall processes of animal experiments. Representative micro-CT images (B), representative MRI images (C), DHI changes (D), MRI gray (E), and Pfirrmann grades (F) of each group in aged rats at 8 weeks. Representative histological staining images of H&E (H) and SF (I) in aged rats at 8 weeks (scale bar = 500 μm). (G) The histological grades of different groups in aged rats at 8 weeks. Data represent mean ± SD; n = 5 per group; statistical significance was analyzed by one-way ANOVA for (D) and (E), $*p < 0.05$, $**p < 0.01$, $***p < 0.001$, and $****p < 0.0001$, ns: no significance. Statistical significance was analyzed by the Kruskal-Wallis test for (G), as well as $*p < 0.05$ and $***p < 0.001$ compared to the PBS group.

characteristics of the NP being surrounded by CEP and AF, long-term and high-dose systemic administration (100 mg/kg, administered every other day for 4–8 weeks) is needed to achieve therapeutic effects in these studies [19,20,44]. This approach greatly reduces the effectiveness of drug treatment and greatly increases the risk of drug complications. In this study, we established an anti-senescence hydrogel for the local delivery of quercetin. Fig. 1 showed that the photocrosslinking and injection characteristics of the GPQ hydrogel were suitable for drug delivery to closed tissues. Moreover, dynamic borate bonds between quercetin and PBA were utilized to release quercetin through a responsive manner in a microenvironment with decreasing pH during IVDD. In contrast, a single local injection of a small dose of GPQ hydrogel with low concentration in vivo had favorable long-term therapeutic effects, suggesting a potential strategy for IVDD treatment.

Oxidative stress-induced senescence and replicative senescence, two types of senescence most closely related to IVDD, represent functional declines caused by exogenous stimulation and endogenous injury. Firstly, we verified in a cellular model of oxidative stress that the GPQ hydrogel reduced the expression of senescence markers and the SASP while inhibiting catabolism, restoring extracellular matrix synthesis, and remodeling cellular metabolic homeostasis (Fig. 2). This finding was similar to that of Shi et al., who synthesized Greigite nanozymes to reverse oxidative stress-induced senescence and slow IVDD [43]. Second, we established a replicative senescence model of NP cells with reference to the work of Cheng et al. [41] to further validate the function of the GPQ hydrogel. Similarly, the GPQ hydrogel effectively improved NP cell senescence and restored the balance of cell metabolism (Fig. 3). Unlike the reprogramming strategy of Cheng et al., we delivered senolytic drugs via a hydrogel system, providing a new option for the treatment of replicative senescence. Overall, in this study, we validated the anti-senescence function of the GPQ hydrogel by using two cellular models and comprehensively assessed the effect of the GPQ hydrogel on NP cell senescence.

Needle puncture injury induced IVDD is a classic animal model. However, in recent years, there is still controversy about the needle size for inducing model. In different studies, 18-27G needles have been used to induce IVDD models in rats, and therefore exhibit inconsistent degrees of degeneration [19,33,43]. Keorochana et al. compared the effects of different needle sizes on IVDD in rats, and found that the 18G needle showed significant degeneration at 2 weeks after surgery, while the 20G and 22G needle showed more significant degeneration at 4 and 8 weeks after injury, respectively [45]. Therefore, in this study, we selected a 20G needle to induce IVDD and evaluated the therapeutic effects at 4 and 8 weeks, which is consistent with the selection in the

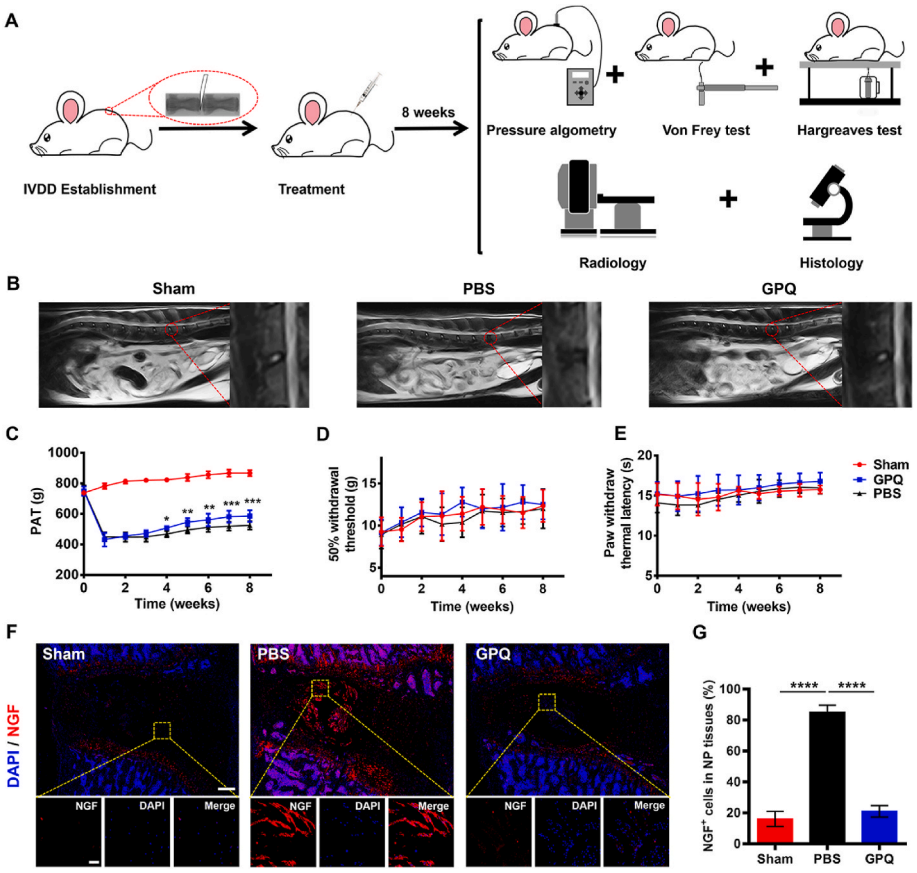

Fig. 7. The GPQ hydrogel effectively reduced LBP caused by IVDD. (A) Schematic illustration showing the entire processes of this animal experiments. (B) Representative T2-weighted MRI sagittal images of lumbar vertebrae in the Sham, GPQ, and PBS groups at 8 weeks. (C–E) Results of PATs, Von Frey test, and Hargreaves test in the sham, GPQ, and PBS groups from 0 to 8 weeks (Sham group: n = 5, GPQ and PBS group: n = 6). (F) Representative fluorescence images of NGF immunostaining (red) at IVD (scale bar = 500 μm above; scale bar = 50 μm below). (G) Quantification of NGF^+ cells in the sham, GPQ and PBS groups (n = 5 per group). Data represent mean ± SD; statistical significance was analyzed by one-way ANOVA; $^*p < 0.05$, $^{**}p < 0.01$, $^{***}p < 0.001$, and $^{****}p < 0.0001$; (C) compared with PBS group.

previous studies [34,46]. To reduce the influence of individual differences on the results, we established different experimental groups in different IVD levels of the same rat tail according to previous studies [29,47], and set the concentration gradients of the treatment groups to determine the optimal concentration for in vivo treatment (Figs. 4 and 5). The 50 μM GPQ group demonstrated better therapeutic outcomes in vivo, especially in the histological results. This is higher than the effective concentration in the cell experiment, indicating that the pathology of the degenerative disc in vivo is more complex and requires higher drug concentrations for treatment. Aging leads to the regression of body function, increasing the difficulty of treating degenerative diseases in the elderly. Considering that IVDD is closely related to age, we further evaluated the long-term therapeutic effect of the GPQ hydrogel in aged rats (Fig. 6). The relevant literature shows that the degree of IVDD in elderly females, especially postmenopausal females, is often more serious than that in males due to factors such as decreased estrogen levels [48–50]. Therefore, in order to exclude the influence of estrogen and other factors on the treatment results, we selected old male rats for the experiment. The results showed that the 50 μM GPQ group demonstrated better treatment effects in both imaging and histological outcomes than the other concentration groups. This finding is similar to the findings of Xing et al., who reported that hydrogels with higher quercetin concentrations could more effectively promote the repair of bone defects in elderly rats [51].

We referred to the previous literature and chose to create a lumbar anterior surgical model to simulate LBP caused by lumbar IVDD [52,53]. Compared with posterior surgery, anterior surgery does not destroy bone structures such as laminae, reducing the impact of lumbar instability caused by damage to bone structure on LBP [3]. Moreover, anterior surgery exposes the IVD more fully with less bleeding, which is conducive to the injection and cross-linking of biological materials. The results showed that the GPQ hydrogel could decrease the expression of NGF in NP tissues and reduce the sensitivity of the degenerated lumbar IVD to mechanical pain. However, in the lower limb mechanical and thermal pain experiments, there were no significant differences among the groups (Fig. 7D and E), as anterior surgery caused the IVD to herniate toward the ventral side without compressing the nerve roots backward; thus, there were no symptoms of lower limb pain, which is consistent with the results of previous studies [53]. In recent years, with the advancement of research, scholars have discovered variations in the impact of gender on diverse diseases and pain. There are differences in pain perception between males and females in IVDD patients [54]. To minimize the potential influence of gender on IVDD and LBP, males were chosen as the subjects of this study. This decision is supported by similar research conducted by other investigators [52,53]. In addition, in future research, it would be beneficial to further investigate the potential treatment differences between males and females of anti-senescence hydrogel.

However, there are still some limitations in this study to be improved. Although needle puncture injury induced IVDD models in rats are frequently used in researches, there are still differences between rat and human IVDD. Compared to human IVDD, rat IVD injury is easier to repair due to its lower nutritional requirements. Therefore, the effects of the GPQ hydrogel on IVDD needs to be further verified in large animals

such as goat, and to explore animal models that more closely resemble humans IVDD. In addition, our study demonstrates that anti-senescence hydrogels can mitigate IVDD and partially attenuate the sensitivity of degenerative discs to mechanical pain in animal models, but their therapeutic effectiveness may be constrained by the degree of disease progression. Although the model does not fully simulate IVDD in humans, there are many similarities in histology and anatomy between rat and human discs. Therefore, the findings of this study suggest that anti-senescence hydrogels may offer a potential approach for the treatment of IVDD, as well as provide insights into treatment strategies for other senescence-associated diseases.

5. Conclusion

In this study, we successfully synthesized PBA-modified gelatin methylacrylyl (GP) and subsequently constructed an injectable hydrogel loaded with quercetin by using the dynamic borate bond between PBA and quercetin. The GPQ hydrogel exhibited pH-responsive release of quercetin. Furthermore, the GPQ hydrogel effectively attenuated the expression of senescence markers and restore metabolic homeostasis in NP cells under conditions of oxidative stress and replicative senescence. In vivo studies revealed that a single local injection of the GPQ hydrogel could maintain disc height and NP tissue structure, and effectively alleviate sensitivity to mechanical pain in IVDD models. Taken together, these findings suggest that treatment with GPQ hydrogel is a promising local therapeutic strategy for IVDD and other senescence-related diseases.

Ethics approval and consent to participate

All animal experiments were approved by the Animal Ethics and Welfare Committee of Southern University of Science and Technology (SUSTech- SL2023030106).

Declaration of interest statement

Decheng Wu is an editorial board member for Bioactive Materials and was not involved in the editorial review or the decision to publish this article. All authors declare that there are no competing interests.

Data availability

Data will be made available on request.

CRediT authorship contribution statement

Wantao Wang: Writing – review & editing, Writing – original draft, Methodology, Conceptualization. **Lei Liu:** Writing – review & editing, Methodology, Conceptualization. **Wenzheng Ma:** Writing – review & editing, Methodology, Conceptualization. **Lei Zhao:** Validation, Software. **Lin Huang:** Validation, Software. **Dan Zhou:** Validation, Software. **Jinghao Fan:** Validation, Software. **Jianru Wang:** Writing – review & editing. **Hongmei Liu:** Writing – review & editing, Supervision, Funding acquisition, Data curation. **Decheng Wu:** Writing – review & editing, Supervision, Funding acquisition, Data curation. **Zhaomin Zheng:** Writing – review & editing, Supervision, Funding acquisition, Data curation.

Acknowledgements

This study was supported by the National Natural Science Foundation of China (82072490 and 21935011) and Shenzhen Science and Technology Innovation Commission (KQTD20200820113012029), and Guangdong Provincial Key Laboratory of Advanced Biomaterials (2022B1212010003).

List of abbreviations

Acronyms	Synonyms
NP	nucleus pulposus
IVD	intervertebral disc
IVDD	intervertebral disc degeneration
LBP	low back pain
AF	annulus fibrous
CEP	cartilage endplate
Col	II type II collagen
GP	phenylboronic acid-modified gelatin methacryloyl
ECM	extracellular matrix
SASP	senescence-associated secretory phenotype
PBA	phenylboric acid
GelMA	gelatin methacryloyl
GPQ	GelMA-PBA-quercetin
APBA	aminobenzeneboronic acid
MES	2-(*N*-morpholino)-ethanesulfonic acid hemisodium salt
EDC	*N*-(3-(dimethylamino)-propyl)-*N*′-ethylcarbodiimide hydrochloride
NHS	*N*-hydroxysuccinimide
PBS	phosphate buffered saline
GelMA-COOH	carboxylated gelatin methacryloyl
^{1}H NMR	hydrogen nuclear magnetic spectrum
DMSO	Dimethyl Sulfoxide
DMEM	Dulbecco's Modified Eagle Medium
CCK-8	cell counting kit-8 assay
PI	propidium iodide
H&E	hematoxylin and eosin
SA-β-Gal	senescence-associated β-galactosidase
qPCR	real-time quantitative reverse transcription PCR
MRI	magnetic resonance imaging
DHI	disc height index
SF	Safranin O-Fast Green
SEM	scanning electron microscopy

(*continued on next page*)

(*continued*)

Acronyms	Synonyms
PATs	pressure algometry thresholds
NGF	nerve growth factor

Appendix A. Supplementary data

Supplementary data to this article can be found online at https://doi.org/10.1016/j.bioactmat.2024.07.031.

References

[1] A. Cieza, K. Causey, K. Kamenov, S.W. Hanson, S. Chatterji, T. Vos, Global estimates of the need for rehabilitation based on the global burden of disease study 2019: a systematic analysis for the global burden of disease study 2019, Lancet 396 (10267) (2021) 2006–2017.

[2] N.N. Knezevic, K.D. Candido, J.W.S. Vlaeyen, J. Van Zundert, S.P. Cohen, Low back pain, Lancet 398 (10294) (2021) 78–92.

[3] F.J. Lyu, H. Cui, H. Pan, K. Mc Cheung, X. Cao, J.C. Iatridis, Z. Zheng, Painful intervertebral disc degeneration and inflammation: from laboratory evidence to clinical interventions, Bone Res. 9 (1) (2021) 7.

[4] S.M. Eisenstein, B. Balain, S. Roberts, Current treatment options for intervertebral disc pathologies, Cartilage 11 (2) (2020) 143–151.

[5] F. Wang, F. Cai, R. Shi, X.H. Wang, X.T. Wu, Aging and age related stresses: a senescence mechanism of intervertebral disc degeneration, Osteoarthr. Cartil. 24 (3) (2016) 398–408.

[6] S. Roberts, E.H. Evans, D. Kletsas, D.C. Jaffray, S.M. Eisenstein, Senescence in human intervertebral discs, Eur. Spine J. 15 (Suppl 3) (2006) S312–S316. Suppl 3.

[7] J. Dowdell, M. Erwin, T. Choma, A. Vaccaro, J. Iatridis, S.K. Cho, Intervertebral disk degeneration and repair, Neurosurgery 80 (3s) (2017) S46–s54.

[8] S. He, N.E. Sharpless, Senescence in health and disease, Cell 169 (6) (2017) 1000–1011.

[9] E.J. Novais, B.O. Diekman, I.M. Shapiro, M.V. Risbud, p16 deletion in cells of the intervertebral disc affects their matrix homeostasis and senescence associated secretory phenotype without altering onset of senescence, Matrix Biol. 82 (2019) 54–70.

[10] N. Vo, H.Y. Seo, A. Robinson, G. Sowa, D. Bentley, L. Taylor, R. Studer, A. Usas, J. Huard, S. Alber, S.C. Watkins, J. Lee, P. Coehlo, D. Wang, M. Loppini, P. D. Robbins, L.J. Niedernhofer, J. Kang, Accelerated aging of intervertebral discs in a mouse model of progeria, J. Orthop. Res. 28 (12) (2010) 1600–1607.

[11] R. Di Micco, V. Krizhanovsky, D. Baker, F. d'Adda di Fagagna, Cellular senescence in ageing: from mechanisms to therapeutic opportunities, Nat. Rev. Mol. Cell Biol. 22 (2) (2021) 75–95.

[12] P. Silwal, A.M. Nguyen-Thai, H.A. Mohammad, Y. Wang, P.D. Robbins, J.Y. Lee, N. V. Vo, Cellular senescence in intervertebral disc aging and degeneration: molecular mechanisms and potential therapeutic opportunities, Biomolecules 13 (4) (2023) 686.

[13] P. Patil, Q. Dong, D. Wang, J. Chang, C. Wiley, M. Demaria, J. Lee, J. Kang, L. J. Niedernhofer, P.D. Robbins, G. Sowa, J. Campisi, D. Zhou, N. Vo, Systemic clearance of p16 -positive senescent cells mitigates age-associated intervertebral disc degeneration, Aging Cell 18 (3) (2019) e12927.

[14] H. Che, J. Li, Y. Li, C. Ma, H. Liu, J. Qin, J. Dong, Z. Zhang, C.J. Xian, D. Miao, L. Wang, Y. Ren, p16 deficiency attenuates intervertebral disc degeneration by adjusting oxidative stress and nucleus pulposus cell cycle, Elife 9 (2020) e52570.

[15] K. Pallauf, G. Rimbach, Autophagy, polyphenols and healthy ageing, Ageing Res. Rev. 12 (1) (2013) 237–252.

[16] M.R. de Oliveira, S.M. Nabavi, N. Braidy, W.N. Setzer, T. Ahmed, S.F. Nabavi, Quercetin and the mitochondria: a mechanistic view, Biotechnol. Adv. 34 (5) (2016) 532–549.

[17] N. Mrvová, M. Kuniaková, V. Knezl, M. Veverka, J. Navarová, R. Nosál, L. Racková, Can semi-synthetic flavonoids return old microglia to their youthful state? Free Radical Biol. Med. (2014) S45.

[18] S.R. Kim, K. Jiang, M. Ogrodnik, X. Chen, X.Y. Zhu, H. Lohmeier, L. Ahmed, H. Tang, T. Tchkonia, L.J. Hickson, J.L. Kirkland, L.O. Lerman, Increased renal cellular senescence in murine high-fat diet: effect of the senolytic drug quercetin, Transl. Res. 213 (2019) 112–123.

[19] D. Wang, X. He, D. Wang, P. Peng, X. Xu, B. Gao, C. Zheng, H. Wang, H. Jia, Q. Shang, Z. Sun, Z. Luo, L. Yang, Quercetin suppresses apoptosis and attenuates intervertebral disc degeneration via the SIRT1-autophagy pathway, Front. Cell Dev. Biol. 8 (2020) 613006.

[20] Z. Shao, B. Wang, Y. Shi, C. Xie, C. Huang, B. Chen, H. Zhang, G. Zeng, H. Liang, Y. Wu, Y. Zhou, N. Tian, A. Wu, W. Gao, X. Wang, X. Zhang, Senolytic agent Quercetin ameliorates intervertebral disc degeneration via the Nrf2/NF-κB axis, Osteoarthr. Cartil. 29 (3) (2021) 413–422.

[21] D.E. Fournier, P.K. Kiser, J.K. Shoemaker, M.C. Battié, C.A. Séguin, Vascularization of the human intervertebral disc: a scoping review, JOR spine 3 (4) (2020) e1123.

[22] Y.L. Lyu, H.F. Zhou, J. Yang, F.X. Wang, F. Sun, J.Y. Li, Biological activities underlying the therapeutic effect of quercetin on inflammatory bowel disease, Mediators Inflamm 2022 (2022) 5665778.

[23] J. Chen, H. Zhu, Y. Zhu, C. Zhao, S. Wang, Y. Zheng, Z. Xie, Y. Jin, H. Song, L. Yang, J. Zhang, J. Dai, Z. Hu, H. Wang, Injectable self-healing hydrogel with siRNA delivery property for sustained STING silencing and enhanced therapy of intervertebral disc degeneration, Bioact. Mater. 9 (2022) 29–43.

[24] R. Zhao, W. Liu, T. Xia, L. Yang, Disordered mechanical stress and tissue engineering therapies in intervertebral disc degeneration, Polymers 11 (7) (2019).

[25] Q. Wei, D. Liu, G. Chu, Q. Yu, Z. Liu, J. Li, Q. Meng, W. Wang, F. Han, B. Li, TGF-β1-supplemented decellularized annulus fibrosus matrix hydrogels promote annulus fibrosus repair, Bioact. Mater. 19 (2023) 581–593.

[26] V.G. Muir, M. Fainor, B.S. Orozco, R.L. Hilliard, M. Boyes, H.E. Smith, R.L. Mauck, T.P. Schaer, J.A. Burdick, S.E. Gullbrand, Injectable radiopaque hyaluronic acid granular hydrogels for intervertebral disc repair, Adv. Healthc. Mater. (2023) e2303326.

[27] P. Li, M. Zhang, Z. Chen, B. Tian, X. Kang, Tissue-engineered injectable gelatin-methacryloyl hydrogel-based adjunctive therapy for intervertebral disc degeneration, ACS Omega 8 (15) (2023) 13509–13518.

[28] C. Ligorio, J.A. Hoyland, A. Saiani, Self-assembling peptide hydrogels as functional tools to tackle intervertebral disc degeneration, Gels 8 (4) (2022).

[29] Y. Liu, J. Du, P. Peng, R. Cheng, J. Lin, C. Xu, H. Yang, W. Cui, H. Mao, Y. Li, D. Geng, Regulation of the inflammatory cycle by a controllable release hydrogel for eliminating postoperative inflammation after discectomy, Bioact. Mater. 6 (1) (2021) 146–157.

[30] Y. Guan, Y. Zhang, Boronic acid-containing hydrogels: synthesis and their applications, Chem. Soc. Rev. 42 (20) (2013) 8106–8121.

[31] K. Yue, G. Trujillo-de Santiago, M.M. Alvarez, A. Tamayol, N. Annabi, A. Khademhosseini, Synthesis, properties, and biomedical applications of gelatin methacryloyl (GelMA) hydrogels, Biomaterials 73 (2015) 254–271.

[32] H. Cheng, Z. Shi, K. Yue, X. Huang, Y. Xu, C. Gao, Z. Yao, Y.S. Zhang, J. Wang, Sprayable hydrogel dressing accelerates wound healing with combined reactive oxygen species-scavenging and antibacterial abilities, Acta Biomater. 124 (2021) 219–232.

[33] W. Chen, H. Chen, D. Zheng, H. Zhang, L. Deng, W. Cui, Y. Zhang, H.A. Santos, H. Shen, Gene-hydrogel microenvironment regulates extracellular matrix metabolism balance in nucleus pulposus, Adv. Sci. 7 (1) (2020) 1902099.

[34] L. Ying, C. Liang, Y. Zhang, J. Wang, C. Wang, K. Xia, K. Shi, C. Yu, B. Yang, H. Xu, Y. Zhang, J. Shu, X. Huang, H. Xing, F. Li, X. Zhou, Q. Chen, Enhancement of nucleus pulposus repair by glycoengineered adipose-derived mesenchymal cells, Biomaterials 283 (2022) 121463.

[35] C.W. Pfirrmann, A. Metzdorf, M. Zanetti, J. Hodler, N. Boos, Magnetic resonance classification of lumbar intervertebral disc degeneration, Spine 26 (17) (2001) 1873–1878.

[36] K. Masuda, Y. Aota, C. Muehleman, Y. Imai, M. Okuma, E.J. Thonar, G. B. Andersson, H.S. An, A novel rabbit model of mild, reproducible disc degeneration by an anulus needle puncture: correlation between the degree of disc injury and radiological and histological appearances of disc degeneration, Spine 30 (1) (2005) 5–14.

[37] A. Lai, J. Gansau, S.E. Gullbrand, J. Crowley, C. Cunha, S. Dudli, J.B. Engiles, M. Fusellier, R.M. Goncalves, D. Nakashima, J. Okewunmi, M. Pelletier, S. M. Presciutti, J. Schol, Y. Takeoka, S. Yang, T. Yurube, Y. Zhang, J.C. Iatridis, Development of a standardized histopathology scoring system for intervertebral disc degeneration in rat models: an initiative of the ORS spine section, JOR Spine 4 (2) (2021) e1150.

[38] J.S. Kim, J.S. Kroin, X. Li, H.S. An, A. Buvanendran, D. Yan, K.J. Tuman, A.J. van Wijnen, D. Chen, H.J. Im, The rat intervertebral disk degeneration pain model: relationships between biological and structural alterations and pain, Arthritis Res. Ther. 13 (5) (2011) R165.

[39] Z. Dai, C. Xia, T. Zhao, H. Wang, H. Tian, O. Xu, X. Zhu, J. Zhang, P. Chen, Platelet-derived extracellular vesicles ameliorate intervertebral disc degeneration by alleviating mitochondrial dysfunction, Mater. Today Bio 18 (2023) 100512.

[40] M. Wan, E.F. Gray-Gaillard, J.H. Elisseeff, Cellular senescence in musculoskeletal homeostasis, diseases, and regeneration, Bone Res. 9 (1) (2021) 41.

[41] F. Cheng, C. Wang, Y. Ji, B. Yang, J. Shu, K. Shi, L. Wang, S. Wang, Y. Zhang, X. Huang, X. Zhou, K. Xia, C. Liang, Q. Chen, F. Li, Partial reprogramming strategy for intervertebral disc rejuvenation by activating energy switch, Aging Cell 21 (4) (2022) e13577.

[42] S. Lim, S.B. An, M. Jung, H.P. Joshi, H. Kumar, C. Kim, S.Y. Song, J.R. Lee, M. Kang, I. Han, B.S. Kim, Local delivery of senolytic drug inhibits intervertebral disc degeneration and restores intervertebral disc structure, Adv. Healthc. Mater. 11 (2) (2022) e2101483.

[43] Y. Shi, H. Li, D. Chu, W. Lin, X. Wang, Y. Wu, K. Li, H. Wang, D. Li, Z. Xu, L. Gao, B. Li, H. Chen, Rescuing nucleus pulposus cells from senescence via dual-functional greigite nanozyme to alleviate intervertebral disc degeneration, Adv. Sci. 10 (25) (2023) e2300988.
[44] W.J. Zhao, X. Liu, M. Hu, Y. Zhang, P.Z. Shi, J.W. Wang, X.H. Lu, X.F. Cheng, Y. P. Tao, X.M. Feng, Y.X. Wang, L. Zhang, Quercetin ameliorates oxidative stress-induced senescence in rat nucleus pulposus-derived mesenchymal stem cells via the miR-34a-5p/SIRT1 axis, World J, Stem Cell. 15 (8) (2023) 842–865.
[45] G. Keorochana, J.S. Johnson, C.E. Taghavi, J.C. Liao, K.B. Lee, J.H. Yoo, S.S. Ngo, J.C. Wang, The effect of needle size inducing degeneration in the rat caudal disc: evaluation using radiograph, magnetic resonance imaging, histology, and immunohistochemistry, Spine J. 10 (11) (2010) 1014–1023.
[46] Z. Zhu, Q. Yu, H. Li, F. Han, Q. Guo, H. Sun, H. Zhao, Z. Tu, Z. Liu, C. Zhu, B. Li, Vanillin-based functionalization strategy to construct multifunctional microspheres for treating inflammation and regenerating intervertebral disc, Bioact. Mater. 28 (2023) 167–182.
[47] J. Shen, A. Chen, Z. Cai, Z. Chen, R. Cao, Z. Liu, Y. Li, J. Hao, Exhausted local lactate accumulation via injectable nanozyme-functionalized hydrogel microsphere for inflammation relief and tissue regeneration, Bioact. Mater. 12 (2022) 153–168.
[48] Y.X. Wang, J.F. Griffith, H.T. Ma, A.W. Kwok, J.C. Leung, D.K. Yeung, A.T. Ahuja, P.C. Leung, Relationship between gender, bone mineral density, and disc degeneration in the lumbar spine: a study in elderly subjects using an eight-level MRI-based disc degeneration grading system, Osteoporos. Int. 22 (1) (2011) 91–96.
[49] N.A. Manson, E.J. Goldberg, G.B. Andersson, Sexual dimorphism in degenerative disorders of the spine, Orthop. Clin. N. Am. 37 (4) (2006) 549–553.
[50] T. Wang, L. Zhang, C. Huang, A.G. Cheng, G.T. Dang, Relationship between osteopenia and lumbar intervertebral disc degeneration in ovariectomized rats, Calcif. Tissue Int. 75 (3) (2004) 205–213.
[51] X. Xing, H. Huang, X. Gao, J. Yang, Q. Tang, X. Xu, Y. Wu, M. Li, C. Liang, L. Tan, L. Liao, W. Tian, Local elimination of senescent cells promotes bone defect repair during aging, ACS Appl. Mater. Interfaces 14 (3) (2022) 3885–3899.
[52] Z. Li, H. Liu, H. Yang, J. Wang, H. Wang, K. Zhang, W. Ding, Z. Zheng, Both expression of cytokines and posterior annulus fibrosus rupture are essential for pain behavior changes induced by degenerative intervertebral disc: an experimental study in rats, J. Orthop. Res. 32 (2) (2014) 262–272.
[53] A. Muralidharan, T.S.W. Park, J.T. Mackie, L.G.S. Gimenez, A. Kuo, J.R. Nicholson, L. Corradini, M.T. Smith, Establishment and characterization of a novel rat model of mechanical low back pain using behavioral, pharmacologic and histologic methods, Front. Pharmacol. 8 (2017) 493.
[54] A. Tschugg, W.N. Löscher, S. Hartmann, S. Neururer, M. Wildauer, C. Thomé, Gender influences radicular pain perception in patients with lumbar disc herniation, J Womens Health (Larchmt) 24 (9) (2015) 771–776.